東京大学 大学院新領域創成科学研究科

基盤科学研究系物質系専攻

平成 20 年度

修士論文

Phase-change memory effect in cobalt oxides

(コバルト酸化物における相変化メモリ効果)

2008 年 7 月 15 日提出

指導教員：高木　英典　教授　印

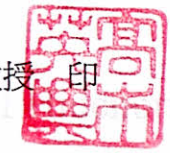

学籍番号：47-66164

谷　雲鵬

Department of Advanced Materials Science
School of Frontier Sciences
University of Tokyo

THESIS

Phase-change memory effect in cobalt oxides

(コバルト酸化物における相変化メモリ効果)

July 15, 2008

Supervisor: Prof. TAKAGI Hidenori

GU Yunpeng

Contents

Chapter 1

Introduction

Phase-change memory, the next generation technology of data storage, has been researched and developed more and more intensively recently. It offers outstanding functional advantages and can exceed limitations that other memory devices are currently experiencing. This technology is believed to become a new trend in the contemporary era with explosive growth of information.

This study aims to develop a new phase-change memory effect using materials in strongly correlated systems, which is a brand-new arena of the phase-change memory. First, superiority of the phase-change memory will be introduced, compared to two commonly used storage devices, hard disk drive and flash memory, as well as their mechanisms.

1.1. Development of data-storage technologies

1.1.1. Hard disk drive

A hard disk drive (HDD) is a non-volatile storage device, which stores data digitally on a magnetic surface of its rotating platter [1]. It was first introduced in 1956 as data storage for an IBM accounting computer [2]. Today a typical HDD is a rigid and fixed drive[1], compared to the floppy disk drive and removable storage devices like memory cards, respectively.

HDDs record data by magnetizing materials on the platter directly, and detect magnetization using a magnetoresistance (MR) read head at first. Later giant magnetoresistance (GMR) came into use as data density increased. The structure of the conventional longitudinal recording system is illustrated in Figure 1.1. The platter is usually made from non-magnetic materials and coated with a thin magnetic layer. This magnetic layer is divided into many small-size magnetic regions consisting of a few hundred magnetic grains, and each of the regions is one magnet bit with a magnetic dipole generating a highly localized field.

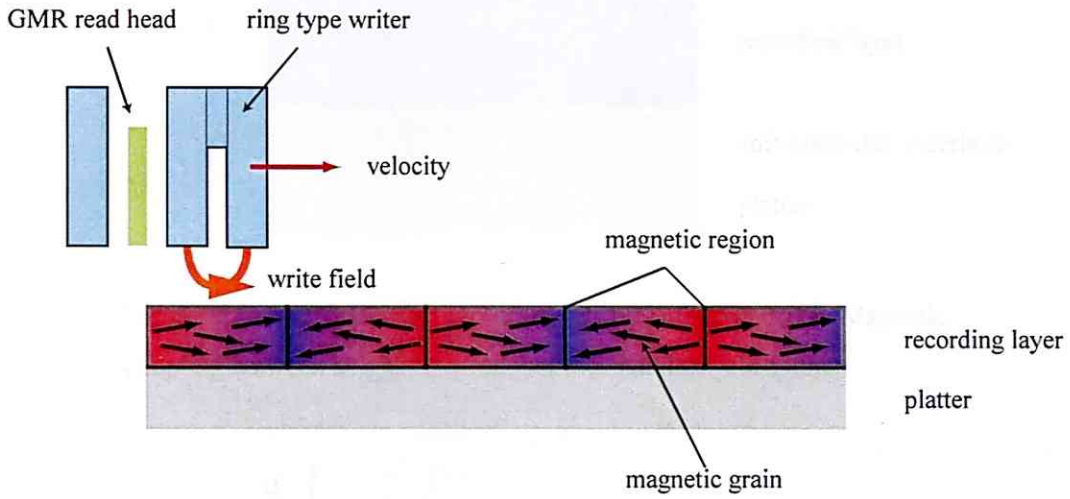

Figure 1.1 Longitudinal recording system in hard disks. Recorded magnets repulse and weaken each other in this conventional system.

[1] Although an external HDD (also known as mobile or portable hard disk) is removable, it is just a normal HDD mounted on a disk enclosure [3]. Thus it works in the same way of the HDD and shares all the problems that an HDD has.

In modern HDDs with extremely large capacity, the size of the magnetic regions is becoming smaller so that at a critical point their magnetization might be lost even due to thermal effects. The newest technology to overcome this barrier is perpendicular recording, which was first shipped in late 2004 [4] and is widely used today. In the conventional longitudinal recording system, magnet bits repulse each other because of their longitudinal alignment. But in the perpendicular recording system (illustrated in Figure 1.2), the coupling between neighboring magnet bits reinforces the stability of their magnetization, and this effect is much more prominent as recording density becomes higher [5], which can be seen Figure 1.3).

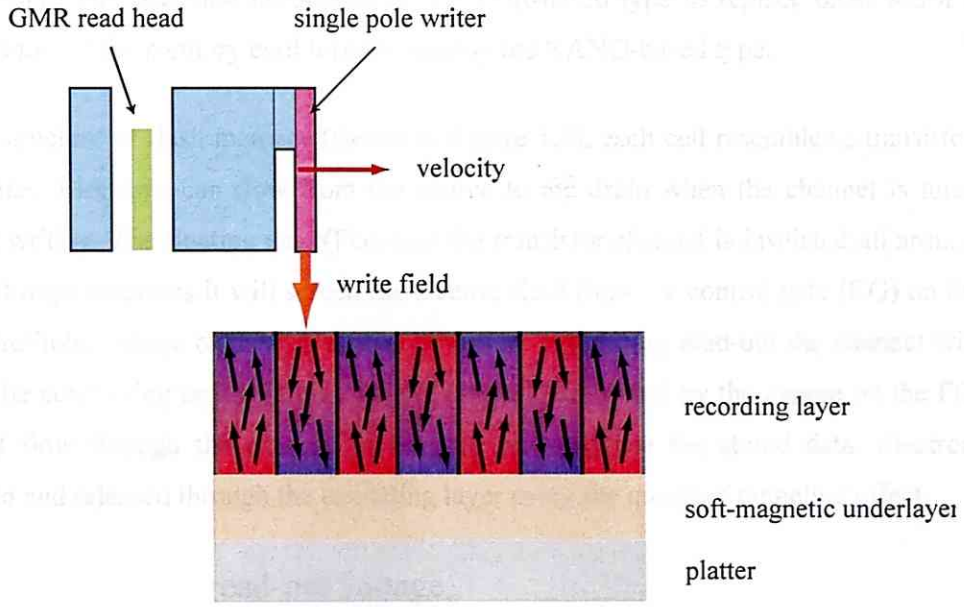

Figure 1.2 Perpendicular recording system in hard disks. Magnetic coupling between neighboring magnet bits stabilizes each other.

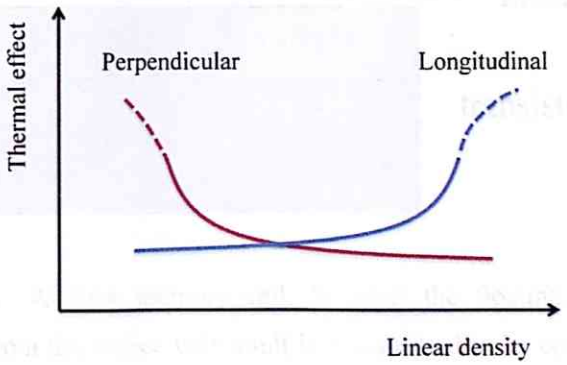

Figure 1.3 Influence of the thermal effect as a function of linear density in both perpendicular and longitudinal recording systems. Perpendicular recording is more suitable for high-density storage.

The main predominance of HDDs compared to other storage devices is their large capacity. But meanwhile several mechanical problems have become important, such as power consumption, audible noise, shock resistance, and especially contamination which can cause data loss. Thus HDDs are more suitable for mass storage rather than portable use.

1.1.2. Flash memory

Flash memory is non-volatile computer memory which stores information in arrays of memory cells made from floating-gate transistors [6]. It was invented by Dr. Fujio Masuoka in 1984 [7], and was first introduced in the NOR-based type to replace older ROM chips. Today most of the memory card formats employ the NAND-based type.

In the structure of flash memory (shown in Figure 1.4), each cell resembles a transistor with two gates. Electrons can flow from the source to the drain when the channel is turned on during writing. The floating gate (FG) near the transistor channel is insulated all around, and when it traps electrons it will screen the electric field from the control gate (CG) on the top. The threshold voltage of the cell is thus modified, and during read-out the channel will turn out to be conducting or insulating, which is in turn controlled by the charge on the FG. The current flow through the channel is detected to reproduce the stored data. Electrons are injected and released through the insulating layer using the quantum tunneling effect.

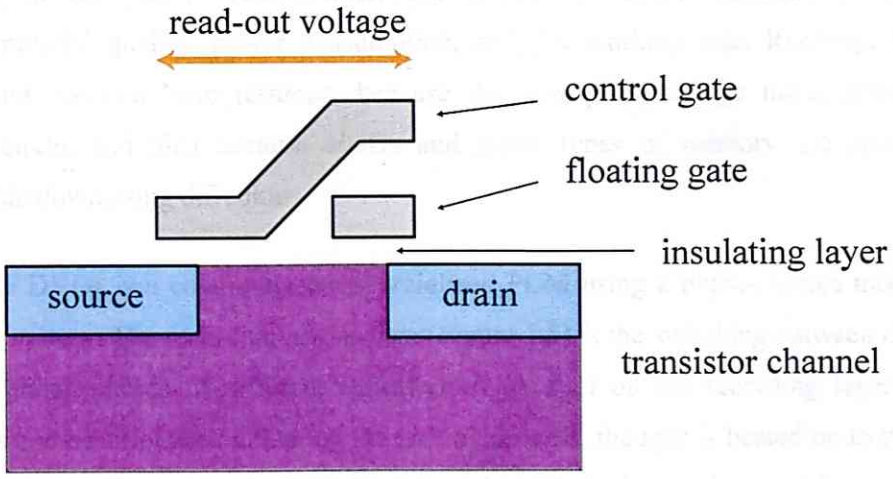

Figure 1.4 A flash memory cell. Whether the floating gate traps electrons from the source will result in the channel to be conducting or insulating.

A useful extension of flash memory is to replace hard disks. Flash memory does not have mechanical problems of hard disks, thus the flash-based solid state drive (SSD) is attractive at present considering its usability and mobility but the high cost. However, one main concern towards flash memory is about its finite number of erase-write cycles (normally 10,000 to 100,000) [8]. This phenomenon of memory wear is caused by the burst of voltage across the cell. Another problem is called block erasure that flash memory must be erased an entire block (a number of bytes) at a time, which limits its performance. All these restrictions have prevented further development of flash memory.

1.2. Phase-change memory effect

Phase-change memory (PCM) is a novel type of non-volatile memory, belonging to the series of upcoming memory models. PCM offers higher performance than other types of recording devices, including flash memory and conventional hard disks. Its mechanism is based on the phase-change memory effect, a switching phenomenon between different phases, or states, with applications of heat. Today PCM is mainly designed to replace flash memory.

The history of phace-change memory effect dates from 1960s when it was firstly developed as an electric field induced phase-change effect in some disordered semiconductors [9], and later the optical phase-change effect in chalcogenide glasses was explored as a potential memory effect [10]. In early years, several obstacles prevented the commerciallization process of PCM such as material quality, power consumption, and the working rate. Recently, however, interest and research have resumed, because the new phase-change material has a fast working circle, and also because HDDs and many types of memory are encountering lithographic downsizing diffculties.

Rewritable DVDs is a commonly commercialized PCM using a phase-change medium, the Ge-Sb-Te system. The recording mechanism (Figure 1.5) is the switching between crystalline and amorphous phases of different reflectivities. A spot on the recording layer of discs represents one bit information. During the writing process, the spot is heated up to its melting point and it transforms to an amorphous (or glass-like) phase when quickly cooled. By heating the amorphous phase up to its crystallization point but lower than the melting point, it changes back to the initial crystalline phase. The amorphous phase has a low reflectivity and represents binary zero, while the crystalline phase has a high reflectivity thus is binary one. This switching idea makes the basis of the PCM effect. The structure of the amorphous phase is still controversial and recent studies have shown that the amorphous phase contains a long-range ordering [11] [12] [13].

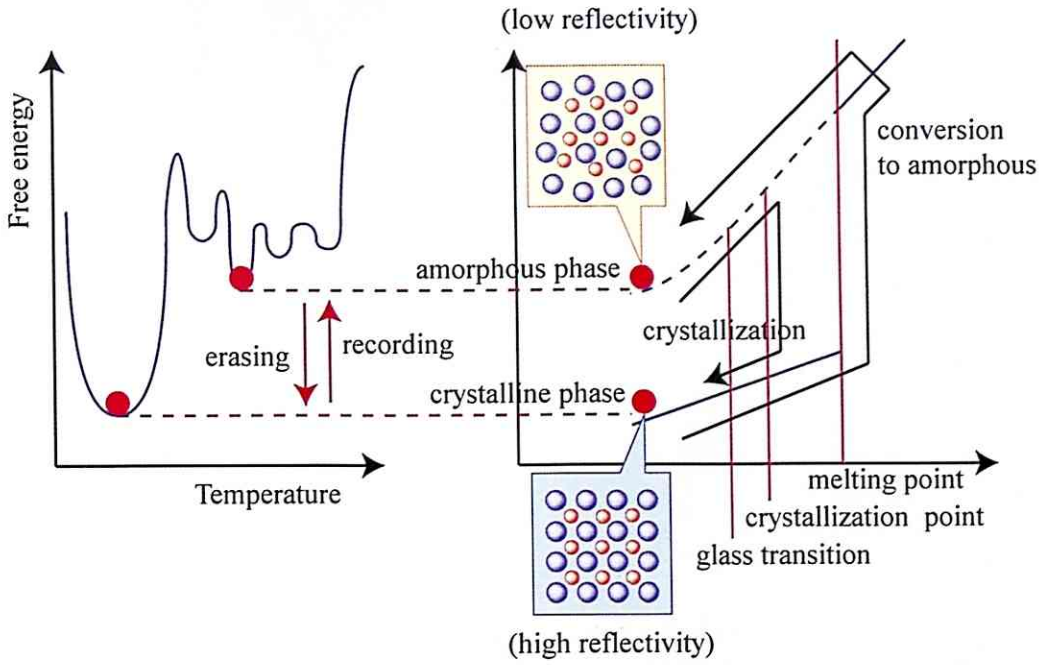

Figure 1.5 Mechanism of the phase-change memory effect. It switches between the amorphous and the crystalline phases with different reflectivities.

The most important characteristic of PCM is that it stores information in forms of the structure, not electrons, which enables it to guarantee data retention for years. This structural recording mechanism also makes PCM much securer and a higher resistance to magnetic fields, electric fields, and even radiation, whereas magnetoelectric devices are susceptible to data corruption. Moreover, the single memory element of PCM can be switched 500 times quickly and rewritten without erasing a whole block of cells [14], and the lifetime of PCM is about 100 million write cycles so that it is far more durable than flash memory [14]. Temperature sensitivity probably seems to be the biggest drawback of PCM, but a recent announcement showed that it could be stable at elevated temperatures [14]. According to a more recent advance, the capacity of PCM has been doubled by adding two new partially crystalline states [15].

1.3. Strongly correlated systems and phase-control methods

Like in the rewritable DVDs, phase transitions usually lead to distinct changes of physical properties. If such phases can be properly controlled, a PCM effect can be expected. From this viewpoint, strongly correlated systems have been chosen to develop a novel PCM effect.

Strongly correlated systems refer to materials in which the electron correlation is large enough so that it cannot be ignored, compared to other systems that can be well described by simple one-electron theories. These compounds usually include transition metal oxides or rare earth series with incompletely filled *d*- or *f*-shells respectively. Charges of the strongly localized *d*- or *f*-electrons cannot be fully shielded by the nucleus, resulting in a strong Coulomb interaction.

It is this correlation effect that makes strongly correlated systems show unusual or complex magnetic and electronic behaviors, such as metal-insulator transitions, high-temperature superconductors, MR and other properties which are technologically useful today. Typically, strongly correlated materials display such colorful properties by undergoing some phase transitions, and the transitions are responsible to external factors like electric fields, magnetic fields, pressure or temperature.

Among these materials, transition metal oxides (TMO) with a perovskite structure display fascinating properties with a variety of electronic phases. In order to apply such properties to practical use, different phases should be properly controlled and induced by some realizable method. One conventional phase-control method is chemical substitution, which is to dope electrons or holes into the system or to change the structure or the band width. Apparently, it is not reversible and not suitable for a memory effect. Another way is the external-field control. In this situation, however, transitions are usually brought at very low temperatures, or fields of extremely large magnitude need to be applied to cause the transitions. Since special equipments are required to perform a field-induced phase control, it is not an appropriate method for actual applications.

As discussed above, a phase-control method providing in-situ phase transitions has become a key to realize the PCM effect. An intrinsic factor, disorder, has been chosen to develop a novel phase-control process. In TMO, disorder can be some structural defects like impurities or vacancies, or a random distribution of some ions in crystals. In rewritable optical discs, phase-change effect is realized by switching between crystalline and amorphous states. By analogy, a disordered phase could be the amorphous state of impurities or vacancies in TMO.

It is expected that different degrees of disorder (or different types of ordering) can affect the properties distinctly especially in strongly correlated systems. Hence, to realize the phase-change control of the disorder in the system will be a promising way. In addition, since a typical PCM works instantly with heat, the control of ordering can also be performed simply by heat treatment, which is an in-situ switching process according with the need of memory applications.

1.4. Cobalt oxides RBaCo$_2$O$_{5.5}$

Cobalt oxides have been focused on in this study to develop such a PCM effect. The layered oxygen-deficient cobalt oxides with a general formula RBaCo$_2$O$_{5+\delta}$ (R for rare earth) recently have attracted much attention due to their intriguing magnetic and transport properties. Especially compounds with $\delta = 0.5$ show unique behaviors as a function of temperature; a resistivity change and magnetic transitions from a paramagnetic (PM) phase to a ferromagnetic-like state (FM) with a spontaneous magnetic moment, followed by antiferromagnetic (AFM) ordering at low temperature [23]. It is argued that such a variety of magnetic phases is associated with the ordering of oxygen vacancies in their structures. The vacancy ordering gives rise to a one-dimensional alternate stacking of low-spin Co^{3+} and intermediate-spin Co^{3+} along the b-axis.

If the disorder is introduced into this vacancy ordering, the magnetism will change distinctly from that of the ordered phase. Such a switching of magnetic properties may be exploited as a novel form of PCM. Thus the PCM effect has been explored in this type of cobalt oxides.

The following text is structured like this: In Chapter 2, experimental details are described. In Chapter 3, a systematic review of RBaCo$_2$O$_{5.5}$ is presented. The crystal structure will be introduced in Section 3.1, magnetic and electric properties will be shown in Section 3.2, and a vacancy order-disorder transition will be explained in Section 3.3. At the end of Chapter 3, strategies for realization of the new phase-change memory effect will be given. In Chapter 4, results of the phase control in RBaCo$_2$O$_{5.5}$ will be discussed, including a study of synthesis conditions and phase-control procedures of PrBaCo$_2$O$_{5.5}$ in Section 4.1, magnetic results in Section 4.2, transport results in Section 0, and structural results in Section 0. In Section 4.5, brief results of the phase control in TbBaCo$_2$O$_{5.5}$ will be presented. Finally in Section 0, perspectives of the phase-change memory effect will be given.

Chapter 2

Experimental

2.1. Sample preparation

Polycrystalline RBaCo$_2$O$_{5+\delta}$ (R = Pr, Tb) samples were synthesized by solid state reaction. Starting materials contained Pr_2O_3 (99.9% up, High Purity Chemicals Co.), Tb_4O_7 (99.99%, Furuuchi Co.), $BaCO_3$ (99.99%, Rare Metallic Co.), and Co_3O_4 (99.9% up, High Purity Chemicals Co.). They were mixed at a stoichiometric ratio and pressed into pellets. The pellets were decarbonated at 900 °C, and then reground and pressed into pellets again. They were finally fired at 1100 °C for 24 h in air to form the phase.

For R = Pr, samples were then oxidized in an oxygen flow at 240 °C for 10 h. To adjust the oxygen content, the sample and excessive amount of powder copper (100 μm, 99.8%, Nilaco Co.) were sealed together in an evacuated quartz tube, annealed at 400 °C and then slowly cooled down to room temperature at a rate of 2 °C/min.

For R=Tb, samples were slowly cooled down to room temperature at 2 °C/min in the end of the air-synthesis.

2.2. Characterization

2.2.1. Structural analysis

Phase characterization of the polycrystalline samples was performed by a powder X-ray diffractometer (MXP21TA-PO, MAC Science Co.). The radiation source was Cu-$K\alpha$ line λ = 1.54184 Å. The samples were placed on a silicon holder. The voltage and current applied during measurement were 45 kV and 400 mA. Data were collected by a step scanning method.

Lattice parameters were computed from powder X-ray diffraction patterns. Positions of peaks were fitted by eliminating the background and Cu-$K\alpha_1$ peaks, and lattice constants were calculated from obtained d-values. The calculation program was Data Management (Ver. 2.2.4a, MAC Science Co.).

2.2.2. Magnetization measurement

Magnetic susceptibility was measured by a SQUID (Superconducting Quantum Interference Device) magnetometer (MPMS *XL*, Quantum Design). Commercial straws were used as sample holders, and polycrystalline powder was wrapped by Al foil which had a 12 μm thickness. The contribution of Al was negligible compared to the magnetization values of samples.

2.2.3. Resistivity measurement

Resistivity of the polycrystalline samples was measured by a standard four-probe method using a physical property measuring system (PPMS, Quantum Design). Bulk samples were used to perform the measurement. Electrodes were made by gold wires (50 μm thickness) and silver paste, and contract resistance was negligible in the measurement.

2.2.4. Stoichiometric determination

The oxygen content (δ) of the synthesized RBaCo$_2$O$_{5+\delta}$ was determined by an iodometric titration apparatus (808 Titrando and 801 Stirrer, Metrohm). It was reported that iodometric titration method could give good reproducibility and accuracy [16] [17]. Powder samples were dissolved in a flask with dilute hydrochloric acid containing excessive potassium iodide. The 10% (weight ratio) potassium iodide solution was prepared by dissolving KI (99.5%, Wako Co.) in deionized water (air inside the water was removed using nitrogen flow), and the 6 mol/L hydrochloric acid was diluted from a HCl solution (35.0 ~ 37.0%, Junsei Co.).

Co^{3+} and Co^{4+} released by the acid could oxidize I^- in the solution:

$$2Co^{3+} + 3I^- \rightarrow 2Co^{2+} + I_3^-$$
$$Co^{4+} + 3I^- \rightarrow Co^{2+} + I_3^-$$

Totally the following redox reaction took place:

$$2R\mathrm{BaCo_2O_{5+\delta}} + (20+4\delta)\mathrm{H^+} + (3+6\delta)\mathrm{I^-} \longrightarrow$$
$$2R^{3+} + 2\mathrm{Ba^{2+}} + 4\mathrm{Co^{2+}} + (1+2\delta)\mathrm{I_3^-} + (10+2\delta)\mathrm{H_2O}$$

From the formula RBaCo$_2$O$_{5+\delta}$, the oxygen content (δ) balances the charge of cobalt ions (Co^{3+} and Co^{4+}), thus the δ could be calculated by the amount of liberated iodine (I_3^-). The iodine was then determined with the titrating solution, sodium thiosulfate:

$$I_3^- + 2S_2O_3^{2-} \rightarrow 3I^- + S_4O_6^{2-}$$

After dissolving the samples, I_3^- was soon titrated with 0.997 mol/L $Na_2S_2O_3$ to avoid the influence of air. The ending point (EP) was well detected using a metal electrode (604 Combined Pt-ring electrode, Metrohm). An experimental titration curve is shown in Figure 2.1.

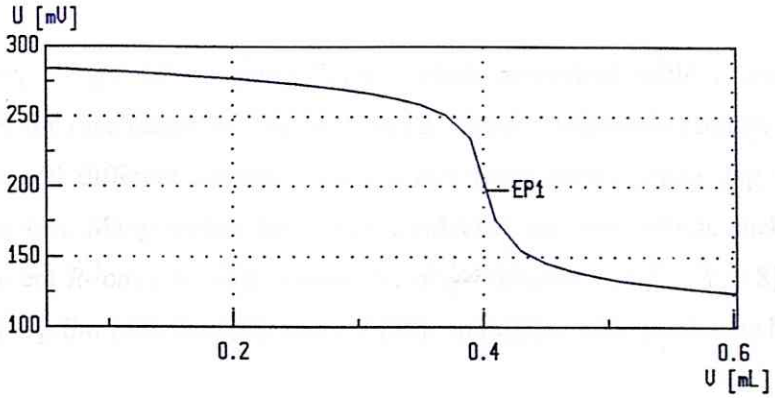

Figure 2.1 Iodometric titration curve of RBaCo$_2$O$_{5+\delta}$. The ending point (EP1) was well detected by the metal electrode.

Chapter 3

Review of RBaCo$_2$O$_{5.5}$

In this chapter, a type of oxygen-deficient cobalt perovskite with a general formula RBaCo$_2$O$_{5+\delta}$ (R for rare earth) will be introduced. These compounds contain different rare earth elements and different oxygen contents, and have shown interesting magnetic and structural properties. Many studies have been conducted into this system, such as structural studies of different R-ions [20] [23], systematic phase diagrams of R = Y [18], Pr [21] [44] [45] [46], Nd [19], Sm [22], Eu [22], and Gd [26], and many other studies including R = La, Tb, Dy, Ho..

RBaCo$_2$O$_{5+\delta}$ with a δ = 0.5 stoichiometry has been particularly focused on because of its special magnetic and electronic behaviors as a consequence of oxygen-vacancy ordering. This work is based on its vacancy ordering, by changing the ordering patterns to a disordered state to control magnetic phases. Before discussing the phase change of the vacancy ordering, let's first take a look at the ordered structure. In the following text, the vacancy ordering in RBaCo$_2$O$_{5.5}$ will be mainly explained.

3.1. Crystal structure of RBaCo$_2$O$_{5+\delta}$

The cobalt oxides, RBaCo$_2$O$_{5+\delta}$ (R for rare earth), are series of layered perovskite compounds with an oxygen-deficient structure. Among their wide range of the oxygen content ($0 \leq \delta \leq 1$), the crystal structure at the point of $\delta = 0.5$ is shown in Figure 3.1. Generally in this oxygen-deficient perovskite structure, A-site cations are ordered R and Ba ions, and B-site polyhedra are [CoO$_6$] octahedra and [CoO$_5$] pyramids. The mean valence of Co ions as well as the ratio of [CoO$_6$]/[CoO$_5$] depend on the oxygen stoichiometry, and layers are stacked along the c-axis in order of [RO_δ]-[CoO$_2$]-[BaO]-[CoO$_2$]-[RO_δ]. As a result, the unit cell of the cubic perovskite (which contains only one polyhedron) is doubled along the c-axis, and the crystal structure of RBaCo$_2$O$_{5+\delta}$ can be represented as tetragonal symmetry with an $a_p \times a_p \times 2a_p$ unit cell (a_p for the cell parameter of the cubic perovskite) [23], by assuming all the polyhedra are equivalent in the structure.

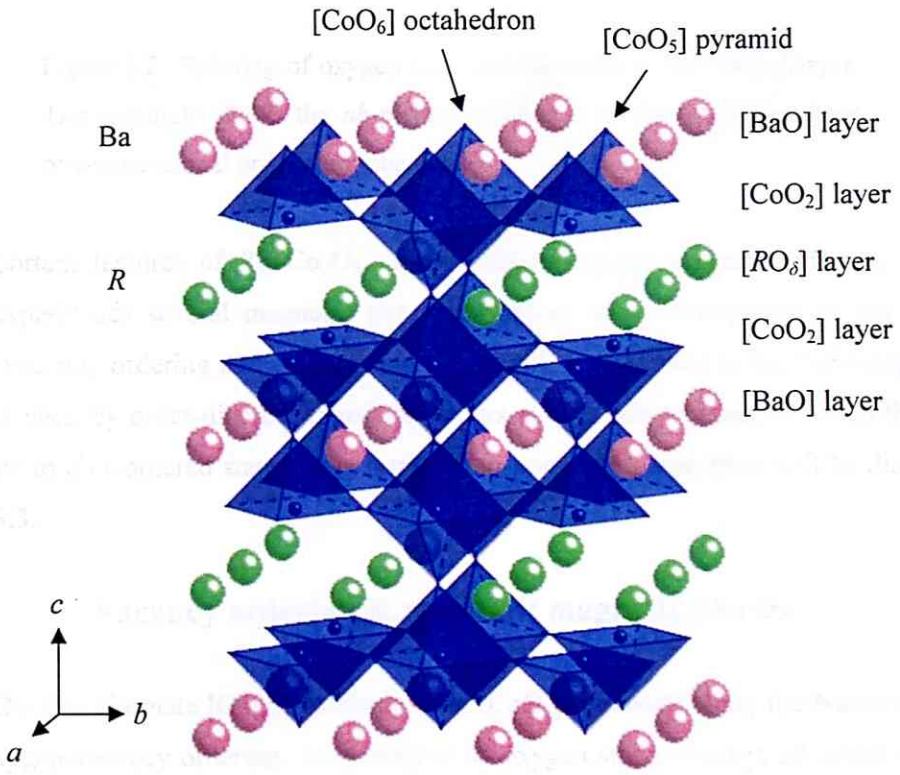

Figure 3.1 Crystal structure of RBaCo$_2$O$_{5+\delta}$ (R for rare earth; $\delta = 0.5$). The alternate ordering of octahedra and pyramids along the b-axis is easily seen.

What makes RBaCo$_2$O$_{5.5}$ so different from other compositions, is its particular oxygen-vacancy ordering. In [RO_δ] layers, half of the oxygen sites are occupied by vacancies due to the oxygen deficiency of δ = 0.5, forming a one-dimensional order in the *ab*-plane. The vacancy ordering in the [$RO_{0.5}$] layers is illustrated in Figure 3.2. Oxygen ions and vacancies alternate along the *b*-axis, and thus the RBaCo$_2$O$_{5.5}$ symmetry is reduced from tetragonal $a_p \times a_p \times 2a_p$ to orthorhombic $a_p \times 2a_p \times 2a_p$ with the unit cell doubled along the *b*-axis.

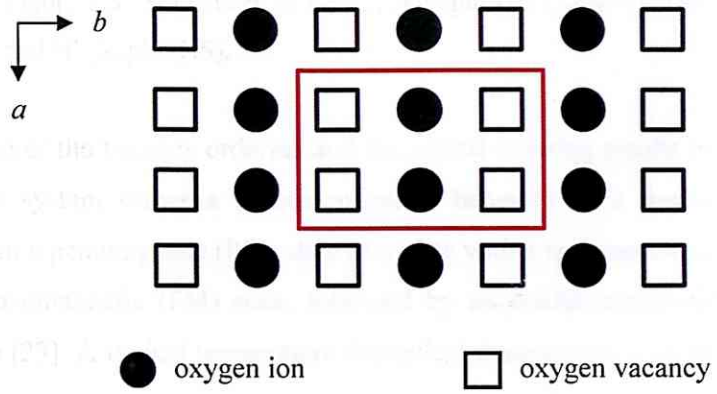

Figure 3.2 Ordering of oxygen ions and vacancies in the [$RO_{0.5}$] layer. The rectangle shows the *ab*-plane in Figure 3.1. The vacancies form one-dimensional order along the *b*-axis.

Two important features of RBaCo$_2$O$_{5.5}$ arise from its oxygen-vacancy ordering. First, the system experiences several magnetic phase transitions as a consequence of the coupling between vacancy ordering and magnetism, which will be explained in the following section. Second, a vacancy order-disorder transition occurs at high temperature, in which the system transforms to a disordered state above a transition point. This transition will be discussed in Section 3.3.

3.2. Vacancy ordering & resultant magnetic phases

RBaCo$_2$O$_{5.5}$ has alternate [CoO$_6$] octahedra and [CoO$_5$] pyramids along the *b*-axis as a result of the oxygen-vacancy ordering. According to its oxygen stoichiometry, all cobalt ions in its structure are trivalent. Spin states of Co^{3+} might not be the same because different coordination environments may favor different spin states. Basically three kinds of spin states exist in Co^{3+}, which are drawn in Figure 3.3. A widely accepted magnetic structure consists of two different spin states of Co^{3+} in the system. At room temperature, Co^{3+} at the octahedral sites is in its low-spin (LS) state with a zero magnetic moment, whereas Co^{3+} at the pyramidal sites is in the intermediate-spin (IS) state. In short, the arrangement of the alternate spin states of Co^{3+}, or the orbital ordering in RBaCo$_2$O$_{5.5}$, is assisted by the oxygen-vacancy ordering.

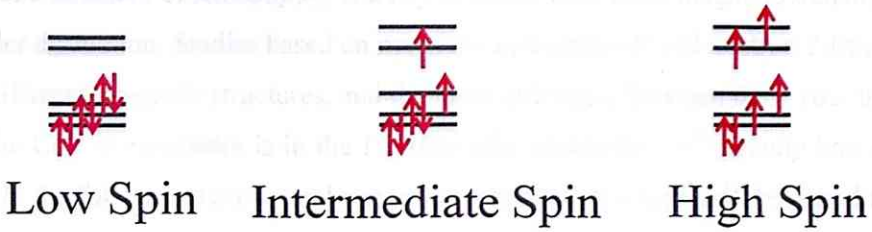

Figure 3.3 Spin states of Co^{3+}: Low spin (LS), Intermediate spin (IS), and High spin (HS).

The coupling of the vacancy ordering and the orbital ordering results in a variety of magnetic phases. The system shows a unique magnetic behavior as a function of temperature: it changes from a paramagnetic (PM) state to a state with a spontaneous magnetic moment, or a so-called ferromagnetic (FM) state, followed by an antiferromagnetic (AFM) state at low temperature [23]. A typical temperature dependent magnetization of RBaCo$_2$O$_{5.5}$ is shown in Figure 3.4.

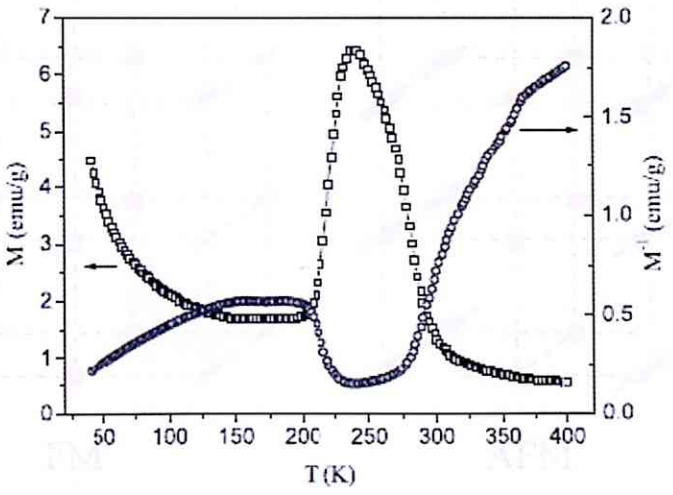

Figure 3.4 The variation of the magnetization for GdBaCo$_2$O$_{4.999}$ in a field of 1 T as a function of the temperature (zero-field cooled and taken on heating) [24].

The magnetic structure of RBaCo$_2$O$_{5.5}$ is a key to understand these magnetic transitions, but it is still under discussion. Studies based on magnetic measurement and neutron diffraction have reported different magnetic structures, and the main difference between these structures is that whether the Co^{3+} in octahedra is in the LS state (the pyramidal Co^{3+} usually has a non-zero moment). In the following text several suggested magnetic structures will be introduced.

Ising-like spin-ladder model

Taskin *et al.* proposed an Ising-like spin-ladder model [25] [26], which is shown in Figure 3.5. The model is based on transport and magnetization measurement using detwinned GdBaCo$_2$O$_{5.50}$ single crystals. In this model, the Co^{3+} in octahedra is in the LS state and the Co^{3+} in pyramids is in the IS state. The magnetic cobalt ions (IS Co^{3+}) form two-leg FM ladders extending along the *a*-axis, and the spinless LS Co^{3+} form nonmagnetic layers. The FM ladders are separated by the nonmagnetic layers along the *b*-axis.

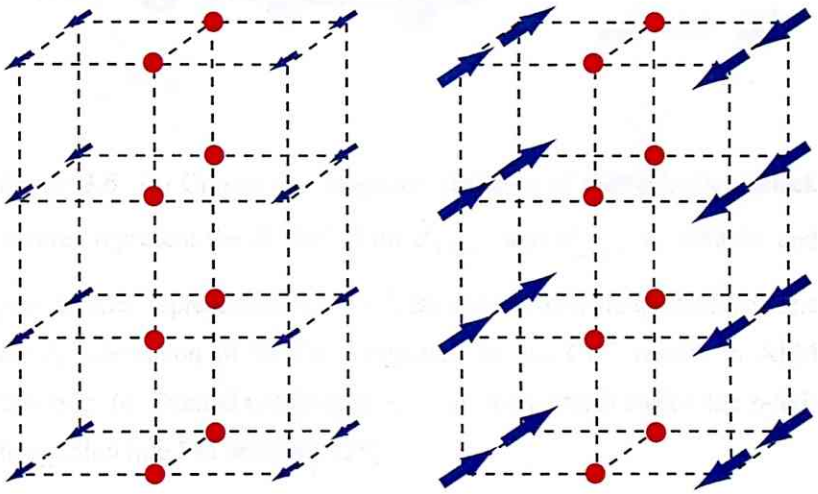

Figure 3.5 Magnetic structure of GdBaCo$_2$O$_{5.5}$ suggested by Taskin *et al.* FM and AFM correspond to the FM and the AFM phases in the present text, respectively. Atomic positions are the same as shown in Figure 3.1. Nodes in the structure are cobalt ions. Arrows represent the IS Co^{3+} with different magnetic moment values. Spheres represent the LS Co^{3+}. [25]

FM spin ordering within ladders is explained by orbital ordering among the IS Co^{3+} shown in Figure 3.6 (a), and in the AFM phase magnetic ordering is caused by a superexchange interaction mediated by the LS Co^{3+} which is illustrated in Figure 3.6 (b). The FM phase, or the AFM-FM transition, can be induced by magnetic fields or temperature. As for the temperature, a mount of the LS Co^{3+} is thermally excited to Co^{2+} and Co^{4+}, and interladder coupling is strongly strengthened enough to form FM ordering, as illustrated in Figure 3.6 (c).

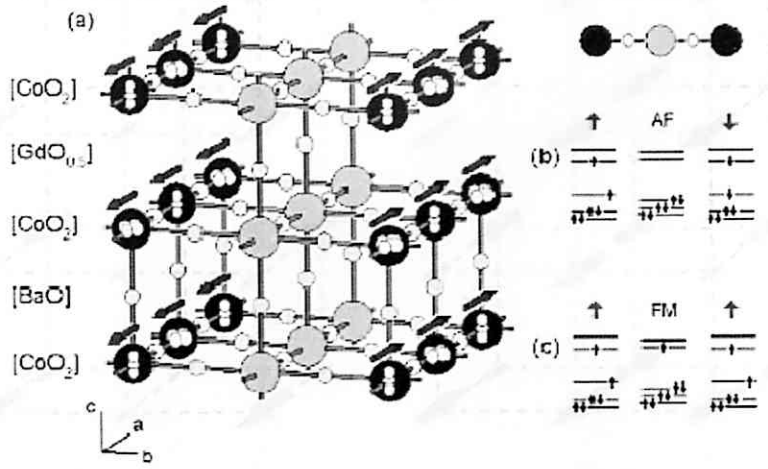

Figure 3.6 (a) Crystal and magnetic structure of $GdBaCo_2O_{5.5}$. Black spheres represent the IS Co^{3+} with $d_{3z^2-r^2}$ and $d_{x^2-y^2}$ e_g orbitals, and gray spheres represent the LS Co^{3+}. Ba and Gd ions are omitted. (b) The *b*-axis interaction of IS Co^{3+} mediated by LS Co^{3+} results in AFM ordering. (c) Excited cobalt ions (Co^{2+} in the picture) switch the *b*-axis interaction into FM ordering. [25]

Ferrimagnetic model

Phakhty *et al.* proposed a ferrimagnetic model [27] [28] shown in Figure 3.7, on the basis of powder neutron diffraction studies of polycrystalline $TbBaCo_2O_{5.5}$. This model does not contain LS Co^{3+}.

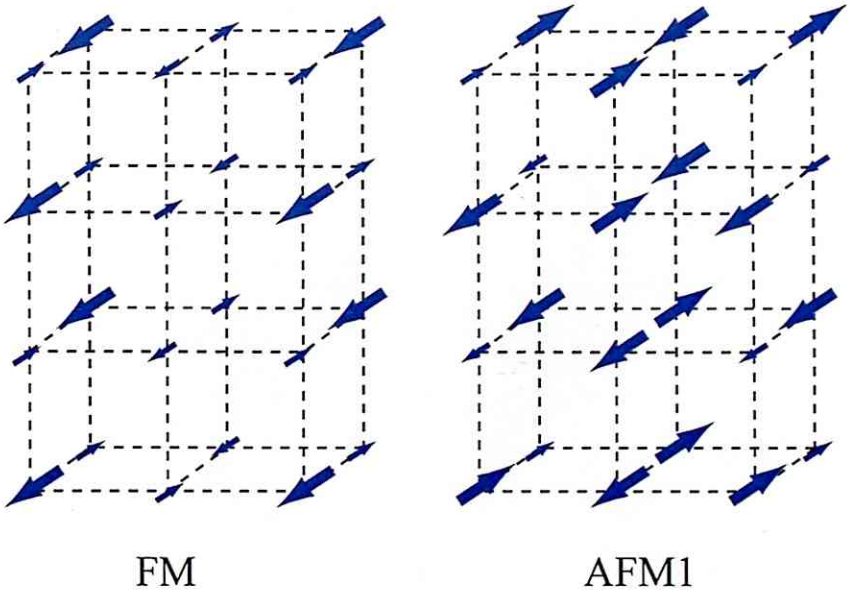

Figure 3.7 Magnetic structure of $TbBaCo_2O_{5.5}$ suggested by Plakhty *et al.* FM corresponds to the FM phase, and AFM1 corresponds to the high-temperature region of the AFM phase in the present text. Atomic positions are the same as shown in Figure 3.1. Nodes in the structure are cobalt ions. Arrows represent the Co^{3+} with different magnetic moment values. [27]

Three phase transitions are identified in this model, including an AFM1-AFM2 transition at low temperature (AFM2 is the low-temperature AFM phase in the present text). In the FM phase, a ferrimagnetic structure is suggested to explain both FM and AFM components observed. As for the AFM1 phase (the high-temperature AFM phase), AFM ordering is along the *c*-axis between ferrimagnetic *c*-planes. Both of the FM and the AFM1 phases are reported to have *Pmma* symmetry with a $2a_p \times 2a_p \times 2a_p$ unit cell, because two distinct cobalt sites (having different values of magnetic moments) exist in pyramids. The AFM2 phase (not presented here) has AFM ordering along the *c*-axis every two ferrimagnetic *c*-planes, thus it has *Pcca* symmetry with a $2a_p \times 2a_p \times 4a_p$ unit cell, and in this phase the octahedra contain those two distinct cobalt sites instead of the pyramids.

Spin-state ordered model

Fauth *et al.* proposed a spin-state ordered (SSO) model [29] from powder neutron diffraction studies of polycrystalline $NdBaCo_2O_{5.47}$, which is shown in Figure 3.8.

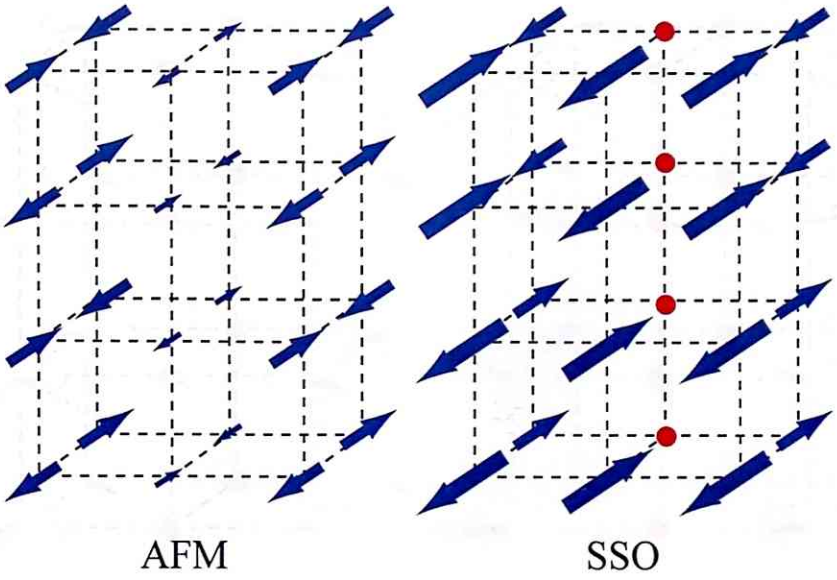

Figure 3.8 Magnetic structure of $NdBaCo_2O_{5.47}$ suggested by Fauth *et al.* AFM and SSO correspond to the FM and the AFM phases in the present text, respectively. Atomic positions are the same as shown in Figure 3.1. Arrows represent the Co^{3+} with different values of magnetic moments. Spheres represent the LS Co^{3+}. [29]

In this model, AFM and SSO phases correspond to the FM and the AFM phases discussed so far, respectively. AFM ordering is adopted to explain the present FM phase, because no FM component was observed in the reported experiment. In the SSO phase, where not all the Co^{3+} in octahedra is in the LS state, both LS and IS Co^{3+} form spin networks of AFM ordering different from its AFM phase, and SSO clustered were observed.

Noncollinear model

Sota *et al.* proposed a noncollinear model [30] [31] shown in Figure 3.9, and it is based on neutron diffraction and NMR studies.

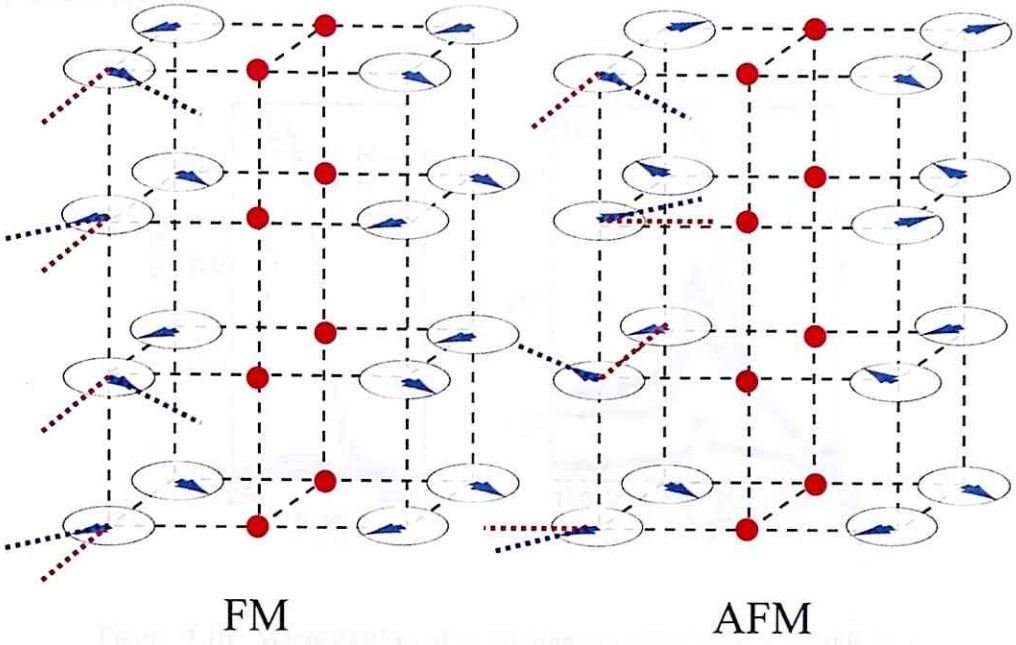

Figure 3.9 Magnetic structure of $TbBaCo_2O_{5.5}$ suggested by Sota *et al.* FM and AFM correspond to the FM and the AFM phases in the present text, respectively. Atomic positions are the same as shown in Figure 3.1. Arrows represent the IS Co^{3+} in pyramids, and spheres represent the LS Co^{3+} in octahedra. [31]

In this model all Co^{3+} in octahedra are in the LS state, and moments of IS Co^{3+} in pyramids are coplanar but canted in the *ab*-plane. In the FM phase, totally a FM moment along the *a*-axis is suggested which is similar to the Ising-like spin-ladder model. But in this case all the moments of the IS Co^{3+} incline from the *a*-axis at a certain angle, and the angle is equal at crystallographic equivalent positions. In the AFM phase, the moments incline from the *a*- and *b*-axes alternately along the *c*-axis, and the nonzero in-plane net moments rotate by 90° every *c*-plane with a $4a_p$ period, forming AFM ordering.

As for the existence of LS Co^{3+}, some NMR experiements have shown that two possible spin states of Co^{3+} exist: one is the LS and the other is the HS or the IS [31] [32] [33]. Considering the strong in-plane anisotropy of magnetization [36] [37] and the large FM moment along the *a*-axis [26] shown in Figure 3.10, it could be reported that the spin-ladder model is more acceptable at present.

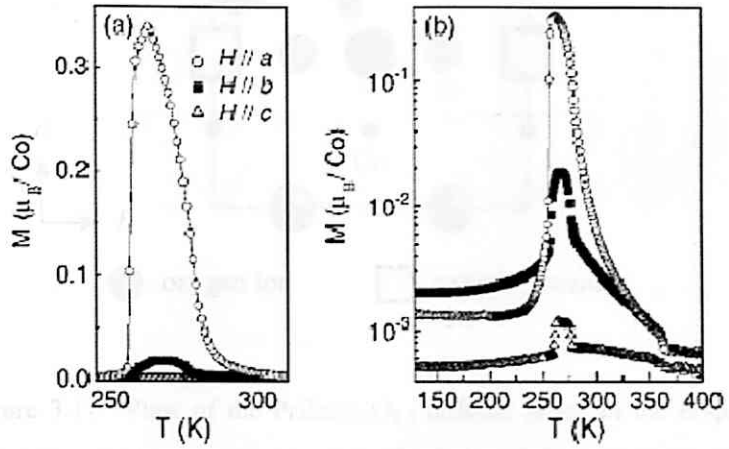

Figure 3.10 Magnetization of a detwinned $GdBaCo_2O_{5.50}$ crystal in a linear (a) and logarithmic scale (b); measurements are done in $H = 0.1$ T applied along one of the crystal axes. The contribution of Gd^{3+} has been subtracted. [26]

3.3. Vacancy order-disorder transition

In some substituted solid solution, alignment of atoms forms an ordered phase at low temperature, and becomes disordered at temperatures higher than a critical point. These transitions of ordering are usually accompanied by structural changes as well as changes of other physical properties like specific heat.

A similar order-disorder transition was also reported in $RBaCo_2O_{5.5}$ (R = Pr) [34] [35], in which the ordering of oxygen vacancies changes at high temperature. This oxygen vacancy order-disorder transition will be first explained in the following text, and then the reported data will be shown.

At room temperature, the crystal structure of $PrBaCo_2O_{5.5}$ can be indexed using the orthorhombic *Pmmm* space group. The simple cubic-perovskite unit cell is doubled along both the *c*-axis due to the alignment of Pr and Ba ions, and the *b*-axis due to the ordering of oxygen vacancies. As introduced previously, the ordered phase can be expressed as the $a_p \times$

$2a_p \times 2a_p$ unit cell. Since the oxygen vacancies form one-dimesional order in $[PrO_{0.5}]$ layers (Figure 3.2), only two oxygen sites can be found in the structure: one is fully occupied by oxygen ions while the other is almost empty (or occupied by oxygen vacancies).

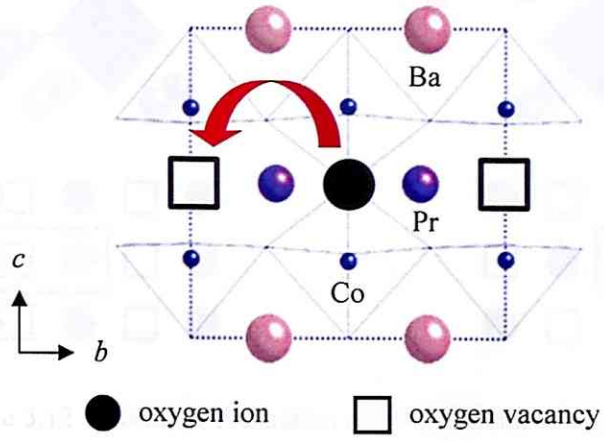

Figure 3.11 View of the $PrBaCo_2O_{5.5}$ ordered phase in the *bc*-plane. The arrow represents a oxygen redistribution at high temperature, where both the two sites have the same possibility containing vacancies (or oxygen ions).

As temperature increases, the occupancy at the oxygen-ion sites decrease and the oxygen-vacancy sites begin to hold oxygen ions. Finally at T_{OD} = 780 K, occupancies of oxygen vacancies at both sites become equivalent. In other words, the system transforms to a disordered state with a random distribution of oxygen vacancies above 780 K. The dislocation is illustrated in Figure 3.11. In this disordered phase, the cubic-perovskite unit cell is no longer doubled along the *b*-axis due to the same occupancy at both sites, resulting in an $a_p \times a_p \times 2a_p$ unit cell. Consequently the transition leads to a crystallographic symmetry change from orthorhombic *Pmmm* to tetragonal *P4/mmm*. The changes of the unit cell and the vacancy ordering can be understood from Figure 3.12.

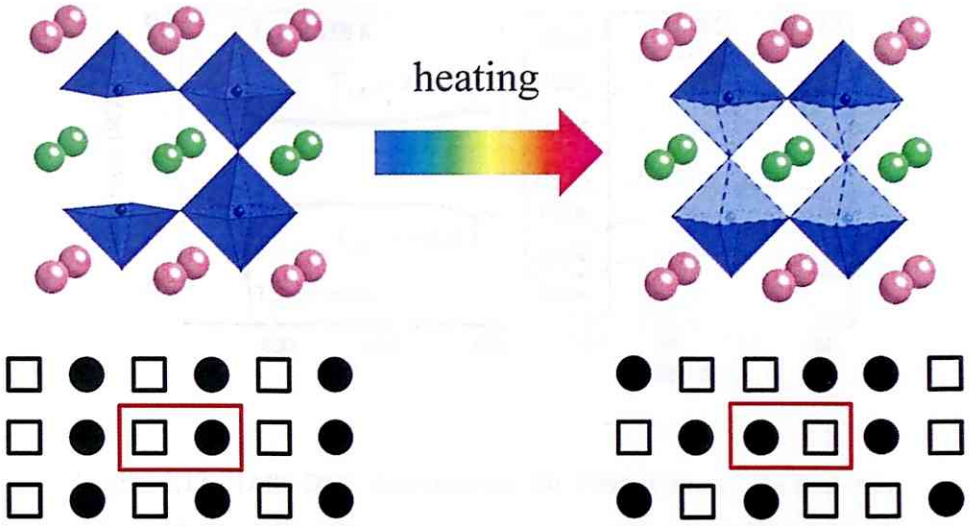

Figure 3.12 Schematic illustration of the structural change in the high-temperature order-disorder transition. The upper figures show that the unit cell changes from $a_p \times 2a_p \times 2a_p$ to $a_p \times a_p \times 2a_p$, where a_p is the cell parameter of the simple cubic perovskite. The bottom figures show that the oxygen-vacancy ordering changes from the alternate alignment to a randomly distributed state, and the red rectangles show the two oxygen sites within the original $a_p \times 2a_p \times 2a_p$ unit cells drawn above.

The reported data of the high-temperature study of $PrBaCo_2O_{5.5}$ are shown in Figure 3.13 and Figure 3.14. The oxygen content of the sample was determined to be 5.48 ± 0.01, and there was no mass loss up to 825 K when heated in an inert atmosphere [34]. Two transition points were detected in the measurement of differential scanning calorimetry (DSC). The first transition around T_{MI} = 340 K corresponds to a metal-insulator transition as reported in other $RBaCo_2O_{5.5}$, for example, $TbBaCo_2O_{5.5}$ [37] [38], and the kink of structural parameters represents a selective spin-state change of Co^{3+} in [CoO_6] octahedra ([38] [39] for R = Tb, [40] [41] for R = Gd, [34] [42] [43] for R = Pr). The second transition was the vacancy order-disorder transition, which can be clearly seen in Figure 3.13 from both DSC and NPD (neutron powder diffraction) data at about 770K to 790 K. The merging of 080 and 400 peaks in the diffraction patterns indicates that symmetry changed from orthorhombic to tetragonal. The evolutions of lattice parameters and oxygen occupancies at the two sites shown in Figure 3.14 also accord with this structural change. In summary, the oxygen vacancies become disordered above the T_{OD}.

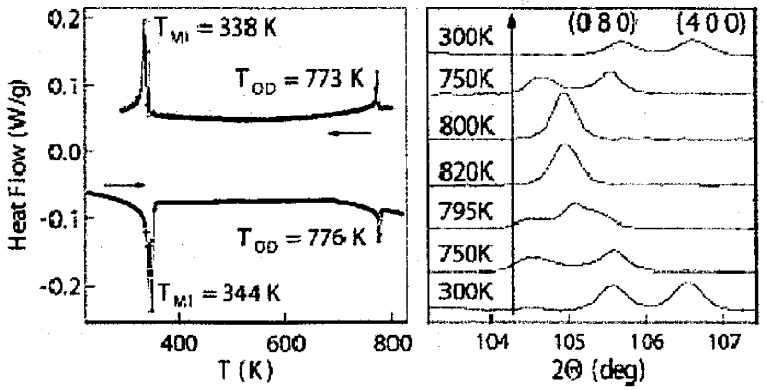

Figure 3.13 Left: DSC measurement for $PrBaCo_2O_{5.48}$. T_{MI} and T_{OD} refer to the metal-insulator transition and the order-disorder transition temperatures, respectively. Right: Temperature dependent evolution of 080 and 400 (orthorhombic indexes) reflections upon heating and cooling (measured with λ = 1.889 Å). [34]

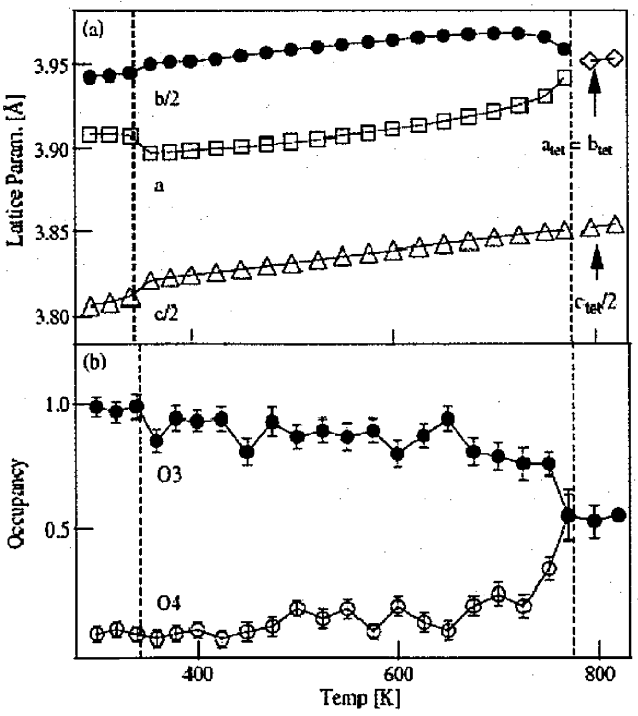

Figure 3.14 Temperature evolution of (a) lattice parameters and (b) oxygen occupancies at the O3 and O4 sites (O3 for the oxygen-ion sites and O4 for the oxygen-vacancy sites in $[PrO_{0.5}]$ layers at room temperature). The slight structural change below 400 K relates to a metal-insulator transition, and the lattice parameters and the oxygen occupancies merge near 800 K in the order-disorder transition. [35]

So far, the most interesting point in the RBaCo$_2$O$_{5.5}$, its particular oxygen-vacancy ordering, has been introduced. In order to tackle the issue of the PCM effect in this system discussed before, a strategy towards the realization of such an effect will be proposed in the following section.

3.4. Strategy towards the new phase-change memory effect

3.4.1. Vacancy-induced magnetic change

This experiment aims to cause a magnetic phase change by introducing vacancy disorder into RBaCo$_2$O$_{5.5}$. Several suggested magnetic structures have been introduced in Section 3.2, and each of them strongly related to the vacancy ordering along the b-axis (Figure 3.1). If this ordered state is broken down, magnetic properties could be strongly influenced, and the change of magnetism may be exploited as a PCM effect.

As explained in Section 3.3, a transition of vacancy ordering exists in RBaCo$_2$O$_{5.5}$ at high temperature. It leads to disordered vacancies along the b-axis, and the structure transforms to a disordered phase compared to its original ordered phase at room temperature. The disordered phase could be obtained by quenching the ordered phase above the transition temperature, which is generally utilized in rewritable optical discs. The quenched phase, or the disordered phase, may exhibit distinct magnetic properties compared with the ordered phase. Thus this vacancy order-disorder transition could be used to cause such a change of magnetism.

3.4.2. Selection of *R*-ions

Among RBaCo$_2$O$_{5.5}$ of various rare earth elements, the selection of R-ions needed to be decided before the experiment. From previous studies [20] [23], RBaCo$_2$O$_{5+\delta}$ samples of various R-ions were synthesized in air at 1100 °C and resulted in different oxygen contents, which are listed in Table 3.1.

Table 3.1 Oxygen contents (δ) of RBaCo$_2$O$_{5+\delta}$ heated in air at 1100 °C. Both of the groups used thermogravimetry to determine the oxygen content.

R	Anderson *et al.* [20]	Maignan *et al.* [23]
Pr	0.68(3)	0.7
Nd	0.62(4)	0.7
Sm	0.54(6)	0.4
Eu	0.52(5)	0.4
Gd	0.42(4)	0.4 (0.5)
Tb	0.41(3)	0.4
Dy	0.36(4)	0.3
Ho	0.25(4)	0.3 (0.4)

It appears that for smaller R-ions (Dy, Ho), the air-synthesized samples have a lower oxygen content ($\delta < 0.4$). While for samples of larger R-ions (Pr, Nd), they have a higher oxygen content ($\delta > 0.6$). Intermediate-sized R-ions (Sm, Eu, Gd, Tb) give the oxygen content near $\delta \sim 0.5$, which is needed by this experiment. In addition, many studied of RBaCo$_2$O$_{5.5}$ have also been done in R = Tb and Gd, because $\delta \sim 0.5$ stoichiometry could be easily obtained in their polycrystalline samples by synthesizing in air only. It is likely that selection of R = Tb or Gd would be the best for this experiment.

However, during the phase-change process in this work, samples need to be heated up to high-temperature disordered phases and then quenched to room temperature. As for the small R-ions, it is expected that their $\delta \sim 0.5$ samples need to be synthesized in oxygen flow or even under high-pressure oxygen atmosphere, and the samples should lose the oxygen content at high temperatures. It will result in a lowered stoichiometry in the quenched (disordered) phases. Variations of the chemical composition could not meet the realization of a PCM effect. Thus they are not selected in this experiment. For the intermediate R-ions, their samples might tend to lose the oxygen content as well at such a high temperature. But considering the $\delta \sim 0.5$ phase can be easily obtained as reported studies, R = Tb was tried in this experiment to perform the phase control.

Finally, for the large R-ions, although the oxygen content of their samples need to be adjusted to $\delta \sim 0.5$ after synthesized in air, they can hold the oxygen at temperatures higher than other R-ions, which guarantees no change of the oxygen stoichiometry during the phase-change

process. Therefore they are thought to be appropriate for the PCM effect, and $PrBaCo_2O_{5.5}$ has been chosen to realize this PCM effect. Firstly, it is reported to have such a transition of oxygen-vacancy ordering [34] [35], which has been explained previously in Section 3.3. This vacancy order-disorder transition provides the basis of the phase change in this work. By introducing the disorder into original magnetic ordering, significant variations of magnetic properties are expected (Section 3.4.1). Secondly, as discussed above, $PrBaCo_2O_{5.5}$ can hold the oxygen at high temperatures, which makes the phase change without changing of the chemical composition.

Chapter 4

Magnetic phase control in $R\mathrm{BaCo_2O_{5.5}}$

In this chapter, a magnetic phase control utilizing the order-disorder transition explained previously was proposed. $R\mathrm{BaCo_2O_{5.5}}$ has the vacancy ordering within its *ab*-planes as explained previously, and introducing disorder into the ordered system might affect its properties distinctly. Since such a disordered phase appears at high temperatures, it was expected that the system would preserve this disordered phase upon quenching it to low temperature. This heat-treatment process was just such like that typical phase-change memory works.

The observed results showed that during the phase-control process described above, a change of the vacancy ordering actually had occurred, and magnetic properties also changed significantly from the original state. Thus a new phase-change memory effect was achieved. Experimental results of $\mathrm{PrBaCo_2O_{5.5}}$ will be presented from Section 4.1 to 0, and results of $\mathrm{TbBaCo_2O_{5.5}}$ will be summarized in Section 4.5. Perspectives of this phase-change memory effect will be given at the end of this chapter.

4.1. Synthesis conditions & phase-control procedures

To develop the phase-control process in RBaCo$_2$O$_{5.5}$, annealing conditions for preparation of PrBaCo$_2$O$_{5+\delta}$ (δ = 0.5) were firstly optimized and then PrBaCo$_2$O$_{5.5}$ samples were successfully obtained. As described in Chapter 2, polycrystalline samples of PrBaCo$_2$O$_{5+\delta}$ were synthesized in air using the solid state reaction. After the pre-synthesis, the samples were oxidized in oxygen flow at a low temperature (T = 240 °C). According to the reported synthesis conditions [44], oxygen can gain a sufficient mobility to diffuse easily into the [PrO$_\delta$] layers at low temperatures, and the oxygen absorption reaches to a maximum at about 240 °C. The stoichiometry of the synthesized samples was found to be δ = 0.75(2) from the iodometric titration, and it was confirmed that no impurity phase existed by the powder X-ray diffraction, which can be seen in Figure 4.1.

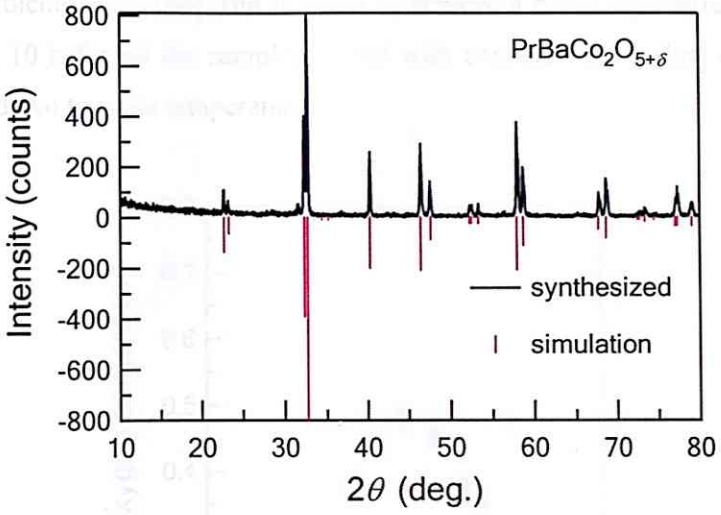

Figure 4.1 X-ray diffraction pattern of the synthesized PrBaCo$_2$O$_{5+\delta}$. The simulation uses PDF#53-0131 (PrBaCo$_2$O$_{5.68}$ with Cu-$K\alpha_1$ λ = 1.5406 Å).

The oxygen content was then adjusted to prepare δ = 0.5 samples. Basically to change the oxygen content in RBaCo$_2$O$_{5+\delta}$, samples should be annealed under specific oxygen pressures and temperatures according to individual working curves. For example, to lower the oxygen content they can be annealed in an inert atmosphere like the argon gas, and this process can be performed either in a furnace or a thermogravimetry [17]. For R = Pr, the oxygen pressure dependent change of the oxygen content at different temperatures has been reported [44]. On the other hand, annealing in oxygen flow or in high-pressure oxygen will increase the δ. Moreover, samples can be sealed in an evacuated ampoule with getter to perform the

reduction, and the final oxygen content is determined either by the calculated amount of getter when annealing at high temperatures [45] [46], or by the annealing temperature when excessive amount of getter added [47] [48].

Since the oxidized $PrBaCo_2O_{5+\delta}$ releases oxygen at $T > 240$ °C [44], metallic copper was used as getter to reduce the oxygen content. A small bulk sample and a large amount of powder copper were sealed together in an evacuated quartz tube, and all the oxygen flowing out of the sample would be absorbed by the getter. The annealing temperature for $\delta = 0.5$ which was reported to be 460 °C [47] did not coincide with the result in this experiment, thus a temperature dependent curve was made, which is shown in Figure 4.2. The annealing temperature was finally determined to be 400 °C, at which the oxygen content is found to be $\delta = 0.48(2)$ by the iodometric titration. It was concluded that for a small amount of powder samples (~ 0.1 g), annealing time longer than 2 h could not produce any further modification to the oxygen stoichiometry [44]. But in order to achieve a better equilibrium, the annealing time was set to 10 h for all the samples sealed with copper, with a slow cooling rate of 2 °C/min, cooled down to room temperature.

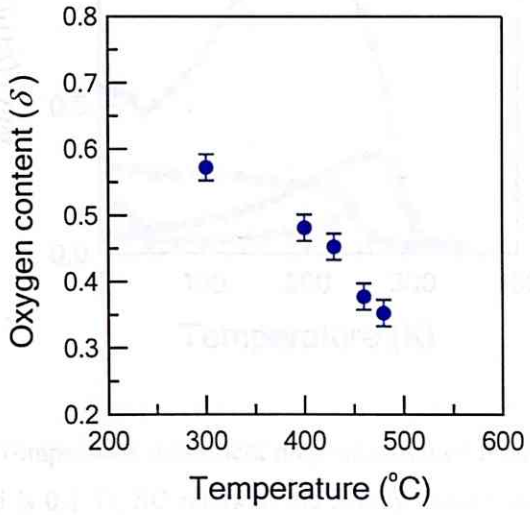

Figure 4.2 Oxygen contents (δ) as a function of reducing temperatures by using copper getter. The oxygen content were determined from the iodometric titration.

As mentioned before, it was expected that the disordered phase could be obtained by quenching the ordered sample above its order-disorder transition temperature ($T_{OD} \sim 780$ K). Because such a vacancy order-disorder transition changes reversibly as fast as it occurs at T_{OD}, the quenching temperature should be higher than T_{OD} but below 825 K where the sample begins to loss its oxygen content [34]. Hence the slowly cooled (SC) sample of $PrBaCo_2O_{5.5}$

was sealed with the argon gas (~ 0.4 bar at room temperature) in a quartz tube, heated up to 550 °C and then quenched into ice water. This quenched sample was named as the rapidly cooled (RC) one. To reveal the disordering effect in this phase-change process, magnetization and resistivity measurement as well as structural analysis were performed for both the SC and the RC samples, and results will be shown in the following sections.

4.2. Magnetic phase change & disordering effect

The magnetization measurement displayed a drastic change of magnetism between the SC and the RC samples. The temperature dependent magnetization presented in Figure 4.3 shows a successive PM-FM-AFM behavior in the SC sample which is typically seen in this system at $\delta = 0.5$, whereas only a reduced peak can be seen in the RC sample.

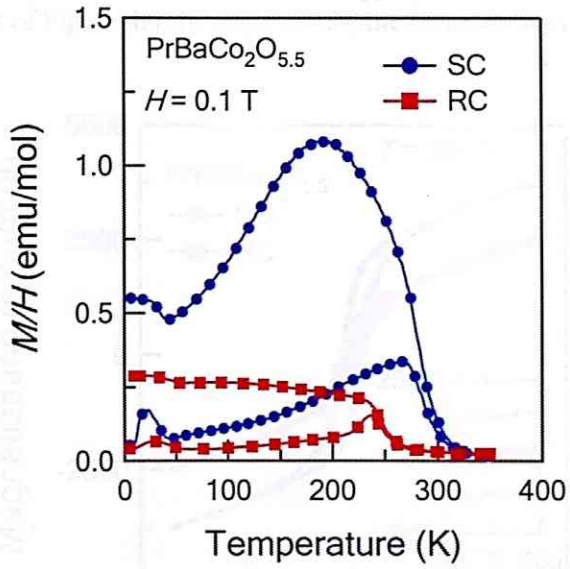

Figure 4.3 Temperature dependent magnetization of $PrBaCo_2O_{5.5}$ (The applied field is 0.1 T). SC refers to the slowly cooled sample and RC refers to the rapidly cooled sample.

As discussed in Section 3.2, in the SC, the FM state was attributed to the linear alignment of the [CoO_5] pyramids (containing IS Co^{3+} of non-zero magnetic moments), as a result of the vacancy ordering [26]. Because the RC was obtained by quenching from a state of disordered vacancies, the long-range vacancy ordering might be broken down. Thus the IS Co^{3+} in the resultant disordered pyramids could not form such a large moment, which led to a reduction of its magnetization.

The temperature dependent magnetization of the RC sample was similar as reported in [45], but with a relatively lower value of magnetization (~ 0.05 μ_B/f.u.) than the reported sample. In that paper the δ = 0.48 sample was quenched from T = 723 K, which is below the order-disorder transition temperature T_{OD} = 780 K. From Figure 3.14 or detailed results in [34], oxygen occupancies at the two sites (discussed in Section 3.3) are 0.33 : 0.73 at T = 750 K, and 0.14 : 0.84 at 600 K. This means that the reported sample did not contain much disorder. In contrast, the RC sample in this experiment was quenched from T ~ 820 K, which is far above the transition temperature, thus it had a higher degree of disorder than the reported one, leading to reduced magnetization results.

To investigate the change of magnetism, magnetization curves were taken at the peak position T = 200 K, and the results are shown in Figure 4.4. The SC exhibited a FM behavior with a small hysteresis. In contrast, the RC shows a superparamagnetic-like behavior, which can be easily seen in the inset of Figure 4.4. In other words, the FM state was suppressed in the RC.

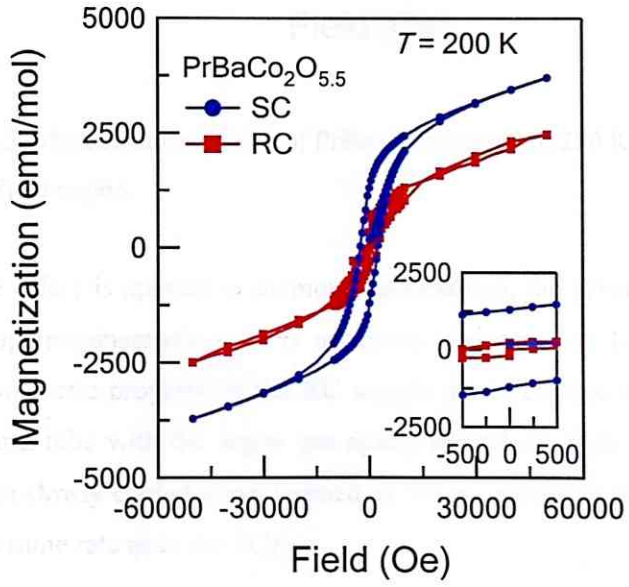

Figure 4.4 Magnetization curves of $PrBaCo_2O_{5.5}$.taken at 200 K. Inset is the low-field region.

Figure 4.5 shows that at a higher temperature $T = 250$ K, the difference in their magnetization curves still remained. The difference can also be seen from their temperature dependent measurement shown in Figure 4.3.

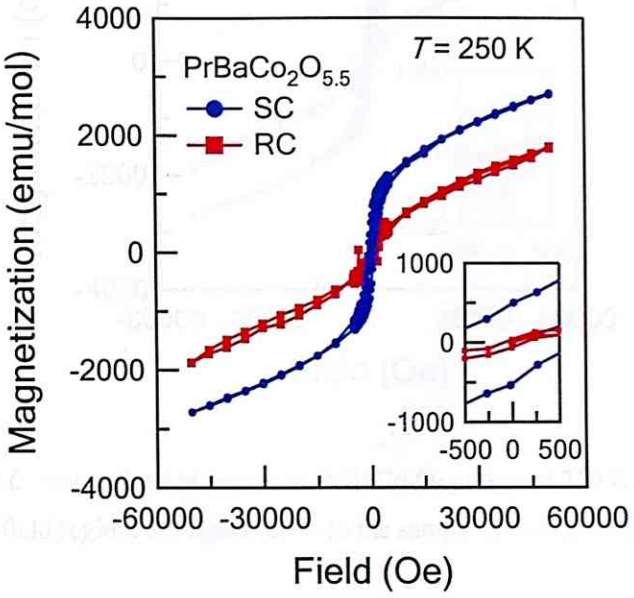

Figure 4.5 Magnetization curves of $PrBaCo_2O_{5.5}$.taken at 250 K. Inset is the low-field region.

If this phase change effect is applied to memory applications, the reversibility between the FM state and the superparamagnetic state is necessary and needs to be tested. In order to check whether the magnetic property of the RC sample could change back, the RC sample was sealed in a quartz tube with the argon gas again, heated up to its formerly quenching temperature, and then slowly cooled down (named as the SC-again) to room temperature at a rate of 2 °C/min (the same rate as in the SC).

As shown in Figure 4.6, RC sample successfully changed back to its initial FM state by performing the slow-cooling process again, thus the recovery of magnetism was confirmed in the SC-again sample.

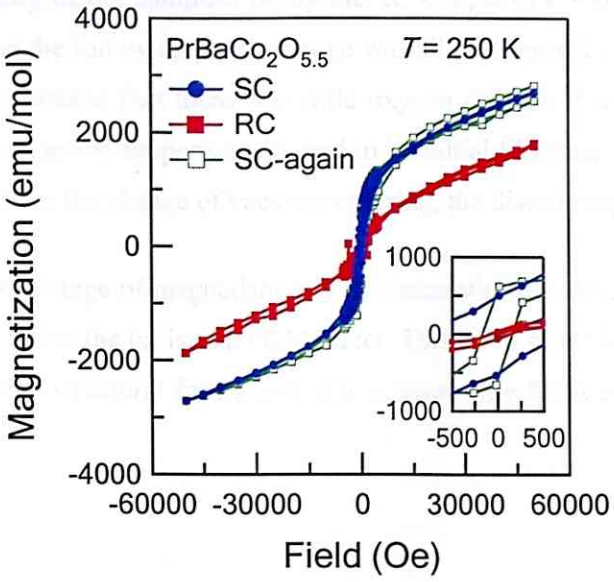

Figure 4.6 Magnetization curves of $PrBaCo_2O_{5.5}$.taken at 250 K. Inset is the low-field region. SC-again refers to the sample slowly cooled again.

In addition, to verify whether its magnetism had fully recovered, temperature dependent measurement of the SC-again sample was performed. The result is shown in Figure 4.7, and it displays that the PM-FM-AFM transitions resumed within the whole temperature range. The difference in susceptibility could be due to errors of weight analysis.

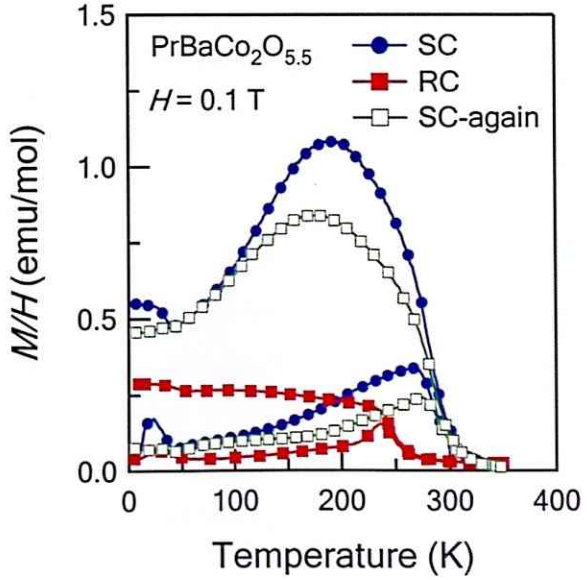

Figure 4.7 Temperature dependent magnetizations of $PrBaCo_2O_{5.5}$.The SC-again sample recovered its magnetism completely.

As for the stoichiometry of our samples, firstly the SC sample of $\delta \sim 0.5$ was obtained with ordered vacancies, and the following phase change was all performed in sealed tubes with the inert gas inside. This ensured that there was little oxygen content change during the whole process. Because the magnetic property recovered to its initial FM state, the magnetic change should mainly result from the change of vacancy ordering, the disordering effect.

After all, based on the change of magnetism and its successful recovery, this magnetic phase change may be proposed as the basis of a PCM effect. This PCM effect is non-volatile since it stores information using structural forms, and it is a novel type PCM effect which works as magnetic memory.

4.3. Change of transport properties

The difference between the SC and the RC samples was also reflected by their transport properties. The temperature dependent resistivity of both samples was taken up to 400 K, and the result is shown in Figure 4.8.

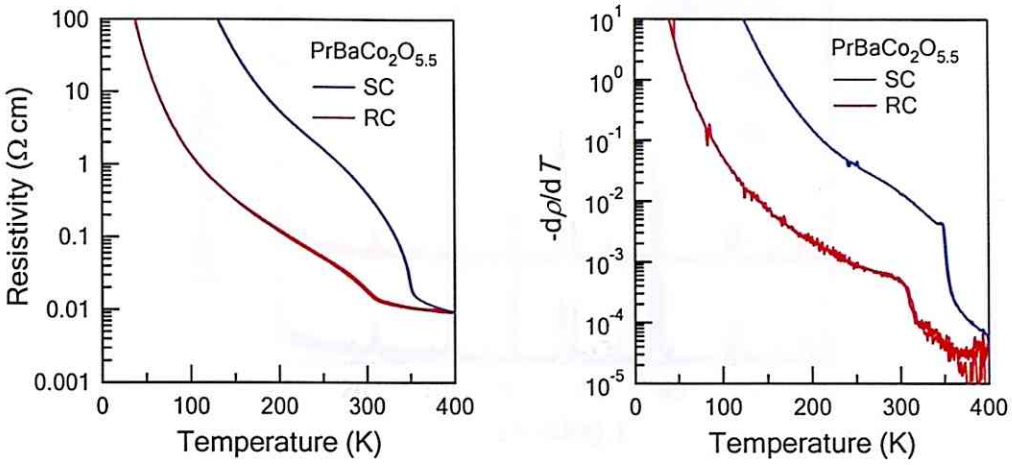

Figure 4.8 Left: Temperature dependent resistivity of $PrBaCo_2O_{5.5}$. Right: The evolution of $d\rho/dT$ as a function of temperature, where ρ represents the resistivity.

From the resistivity measurement, the SC displayed a typical transport behavior of $RBaCo_2O_{5.5}$ including a metal-insulator transition, and the resistivity jump is emphasized in the evolution of $-d\rho/dT$ and was found at T = 350 K. It changed the magnitude of the resistivity from 0.01 Ω·cm to 0.1 Ω·cm. The resistivity jump was also found in the RC but at a lower temperature of T = 310 K, and it was not as sharp as in the SC.

Although the bulk measurement is relatively rough compared with single crystals, from the results the difference in transport behaviors can still be estimated. In the SC, the resistivity jump was very sharp which could be recognized as a metal-insulator transition. But the transition seemed to be broadened in the RC, and the transition point was found to be lower with a more gradual change compared to the SC. This broadened metal-insulator transition might be resulted from the disordered vacancies.

4.4. Structure of the disordered phase

To investigate what happened to the RC sample during the quenching process, structural analysis was performed by the powder X-ray diffraction for both the SC and the RC samples.

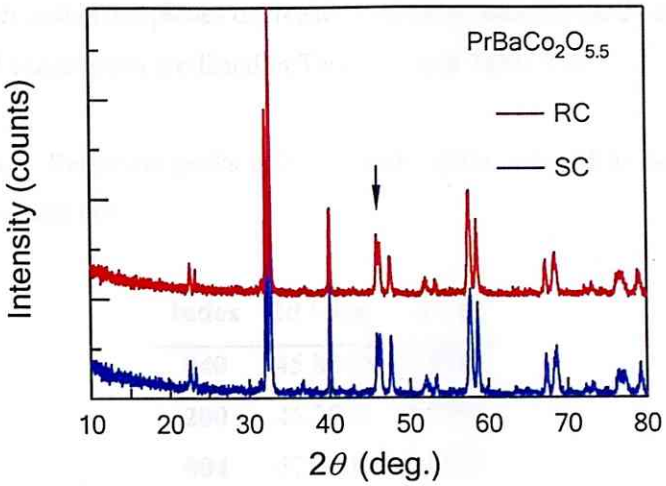

Figure 4.9 X-ray diffraction patterns of $PrBaCo_2O_{5.5}$. The arrow points at the peaks derived from the ordering of oxygen vacancies.

X-ray patterns taken from $2\theta = 10^\circ$ to 80° shown in Figure 4.9 indicates that there was no significant difference between the SC and the RC. However, if the vacancy ordering had changed in the RC, peaks originating from the vacancy ordering might be different from the SC. Thus high-resolution scans were performed at a range from $2\theta = 45^\circ$ to 50°.

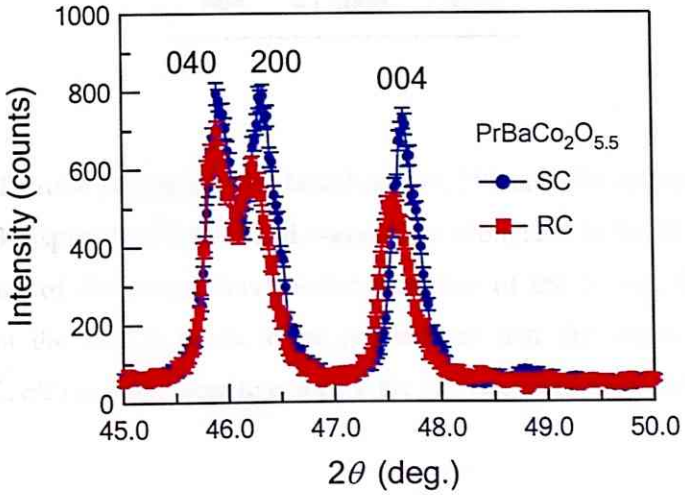

Figure 4.10 X-ray diffraction patterns of $PrBaCo_2O_{5.5}$. The split of 040 and 200 peaks was caused by the vacancy ordering within the *ab*-plane.

Diffraction patterns shown in Figure 4.10 displays that peaks derived from the vacancy ordering have changed in the RC sample. Originally in the SC, 040 and 200 reflections (all indexed in the $a_p \times 2a_p \times 2a_p$ unit cell) split around $2\theta = 46^\circ$ due to the vacancy ordering along the *b*-axis. On the other hand, the two peaks became closer in the RC, which is similar to 080 and 400 peaks shown in Figure 3.13. As 040 and 200 peaks get closed, the difference between (010) planes and (100) planes decreases gradually, making the *b*- and *a*-axes become similar. Positions of these peaks are listed in Table 4.1 and Table 4.2.

Table 4.1 Reflection peaks of $PrBaCo_2O_{5.5}$ (SC), indexed in the $a_p \times 2a_p \times 2a_p$ unit cell

Index	**2θ / deg.**	***d* / Å**
040	45.8800	1.9763
200	46.3000	1.9593
004	47.6400	1.9073

Table 4.2 Reflection peaks of $PrBaCo_2O_{5.5}$ (RC), indexed in the $a_p \times 2a_p \times 2a_p$ unit cell

Index	**2θ / deg.**	**d / Å**
040	45.8400	1.9779
200	46.2000	1.9633
004	47.5000	1.9126

The calculation of lattice parameters was based on 040, 200 and 004 reflection peaks. Results listed in Table 4.3 display that both *a*- and *c*-axes were elongated in the RC phase. In the SC, the lattice constant of the *a*-axis was shorter than that of the *b*-axis. But this difference became shrunk in the RC. It needs to be pointed out that the pseudo cubic perovskite parameters (*a*, *b*/2, *c*/2) are used here to compare the lattice constants of different axes.

Table 4.3 Lattice parameters of $PrBaCo_2O_{5.5}$. Volume was calculated in the unit of pseudo cubic perovskite cells

Phase	a / Å	$\frac{b}{2}$ / Å	$\frac{c}{2}$ / Å	V / Å^3
SC	3.9186	3.9526	3.8146	59.083
RC	3.9266	3.9558	3.8252	59.416

In the structure of $R BaCo_2O_{5.5}$, cobalt ions have two spin states, which has been discussed in Section 3.2. The IS Co^{3+} ions have larger radii than the LS Co^{3+}, thus in the $[CoO_5]$ pyramids Co-O bonds are longer than in the $[CoO_6]$ octahedra. In the SC, the *a*-axis parameter was mainly determined by the ordered octahedra in arrays of the one-dimensional vacancy ordering. Thus the pyramids could only expand along the *b*-axis, leading to a larger lattice constant at the *b*-direction. In contrast, in the RC, since the long-range order of octahedra did not exist any more, disordered pyramids would lead to a significant expansion along the *a*-axis. And this expansion was actually observed in this experiment.

As for the expansion along the *c*-axis, it might be considered as a result of vacancy disordering within the *ab*-plane. Originally in the SC, octahedra and pyramids linked separately along the *c*-axis due to in-plane ordered vacancies. But as the vacancies were no longer ordered in the RC, they had to link to each other randomly, and this looser connection in the space finally led to this *c*-axis expansion. In other words, the ordered phase had a more compact structure than the disordered phase.

The changes of magnetic and transport properties in the RC sample were attributed to this structural change. It is believed that a completely disordered state should have a tetragonal symmetry ($a_p \times a_p \times 2a_p$) with just one peak of the 200 reflection. It seemed, however, that under the present conditions only partial disorder could be obtained, which resulted in a superparamagnetic behavior.

In order to clarify the points discussed so far, a completely disordered phase needs to be obtained through a much faster quenching process, and detailed structural analysis also needs to be performed. In summary, the disorder caused the structural change and thus affected the magnetism.

4.5. Phase control in $TbBaCo_2O_{5.5}$

Besides the study of $PrBaCo_2O_{5.5}$, $TbBaCo_2O_{5.5}$ has been also investigated so as to develop the PCM effect.

Preparations for $TbBaCo_2O_{5.5}$ could be simply obtained from air-synthesis, as discussed in Section 3.4.2. Polycrystalline $TbBaCo_2O_{5.5}$ samples were synthesized by solid state reaction, and slowly cooled down to room temperature at a rate of 2 °C/min. The disordered phase was obtained also by quenching the slowly cooled (SC) sample from a high temperature of T = 500 °C, named as the rapidly cooled (RC) sample. Both the SC and the RC phases were checked by the powder X-ray diffraction, and no impurity phase was confirmed. Magnetic and transport properties of both the SC and the RC samples were measured to reveal the disordering effect.

A similar magnetic phase change was also found in $TbBaCo_2O_{5.5}$. The temperature dependent measurement shown in Figure 4.11 displays typical PM-FM-AFM transitions in the SC sample, but with a much sharper peak compared to the case of $PrBaCo_2O_{5.5}$. While only a broad peak was seen in the RC sample.

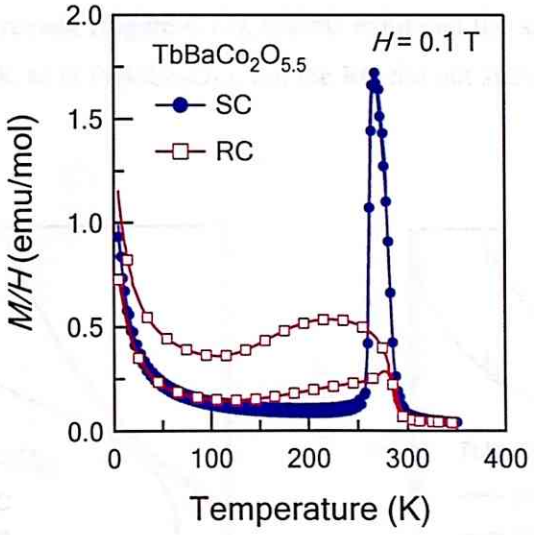

Figure 4.11 Temperature dependent magnetization of $TbBaCo_2O_{5.5}$ (The applied field is 0.1 T). SC refers to the slowly cooled sample and RC refers to the rapidly cooled sample.

Magnetization curves taken at 270 K shown in Figure 4.12 displays a FM behavior with a small hysteresis in the SC. In contrast, the RC showed a superparamagnetic behavior without any hysteresis.

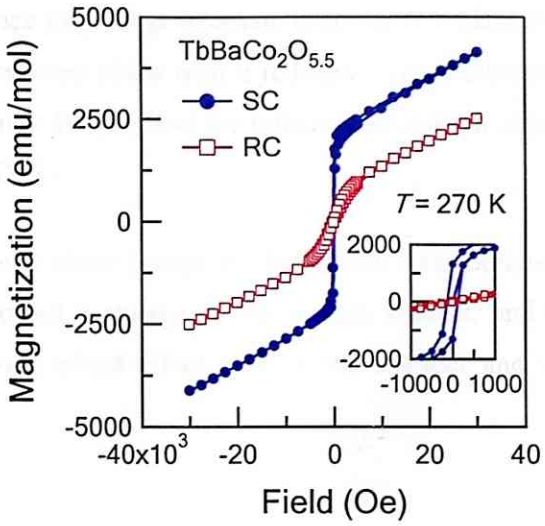

Figure 4.12 Magnetization curves of $TbBaCo_2O_{5.5}$.taken at 270 K. Inset is the low-field region

In the resistivity measurement (Figure 4.13), the SC exhibited the same kind metal-insulator transition at about 340 K as in $PrBaCo_2O_{5.5}$, but the RC did not show any resistivity anomaly up to 400 K.

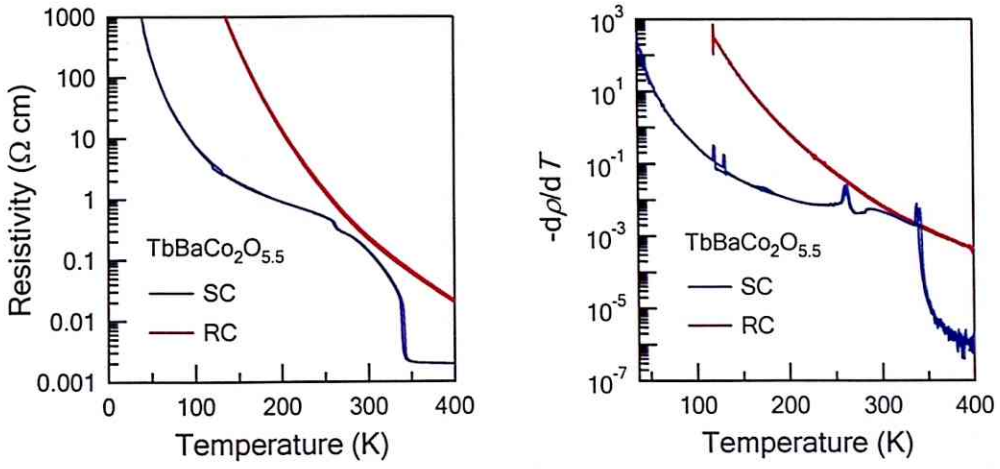

Figure 4.13 Left: Temperature dependent resistivity of $TbBaCo_2O_{5.5}$. Right: The evolution of $d\rho/dT$ as a function of temperature, where ρ represents the resistivity.

However, the study of oxygen stoichiometry showed that the SC sample of $TbBaCo_2O_{5.5}$ had a δ = 0.46(2) composition, while the RC was found to be δ = 0.36(2). Just as discussed previously in Section 3.4.2, $TbBaCo_2O_{5.5}$ tends to lose its oxygen content at high temperatures. If the oxygen content deviates from the optimal value $\delta \sim 0.5$, the vacancy ordering also becomes disordered since long-range alternate ordering is broken down as well. This means that the RC was a disordered phase with a reduced oxygen content. Thus actually a mixed effect of both the vacancy disorder and the influence of oxygen content were observed in the phase change of $TbBaCo_2O_{5.5}$.

In summary, the magnetic phase change in $TbBaCo_2O_{5.5}$ was obtained by heat treatment. But this phase change involved a change of the oxygen content, and the resultant changes of properties were due to a mixed effect of both the disorder and variations of the oxygen content.

4.6. Perspectives of the phase-change memory effect

4.6.1. Advantages over other recording systems

The main characteristic of this PCM effect is that it utilized the structural change between two phases of different magnetic properties. Conventional magnetic recording is based on the directions of spontaneous magnetizations. In contrast, this PCM effect is based on whether the phases have or have not spontaneous magnetizations, which is depended on their structures. Due to this structural recording mechanism, advantages of this PCM effect compared to other recording devices will be discussed below.

- downsizing of systems

First, the recording system can be downsized in this PCM effect. Because this PCM effect is non-volatile, thus magnetic fields are not needed to apply to recording materials during writing or erasing processes, and it is not always necessary to apply magnetic fields like in other magnetic recording systems.

- high density and capacity

Second, conventional recording is based on the directions of magnet moments, and domains require sufficiently large size to stabilize their moment directions, or thermal effects would cause a reversal of moments. But this PCM effect does not need to keep the moment directions, thus the domain size could be further scaled down, and storage of extremely high density and large capacity can be realized in this PCM effect.

- high stability

Third, this PCM effect stores information in the structural form, not using magnetic or electronic, thus it offers high security and stability within magnetic fields, electric fields and even radiation, for example. Apparently magnetic recording systems as well as flash memory are susceptible to data corruption.

4.6.2. Perspectives in RBaCo$_2$O$_{5.5}$

As for the PCM effect in RBaCo$_2$O$_{5.5}$, its working temperature was 550 °C (R = Pr) in this experiment. It is a bit lower than the working temperature of normal phase-change materials, which is 600 °C. Generally, a low working temperature may be preferable for applications of PCM considering power consumption. But a too low working temperature makes the PCM not stable, because the disordered state might become unstable at room temperature. Although the working temperature has not been optimized yet, it is realizable for applications as a PCM effect.

In this experiment, the phase change was not completely since only partially disordered phase had been obtained. It is likely due to the slow cooling rate of the quenching process under present experimental conditions. One way to achieve a more rapid cooling process may be the phase change in a thin-film form. The bulk form sometimes prevents materials from transforming to completely disordered states, but the film form or spots may provide such a rapid cooling rate for this PCM effect. On the other hand, if the disordered phase can be easily obtained, it will take a long time to recover to the ordered phase. In this experiment, the ordered phase has particular vacancy ordering, and even partial changes of the ordering resulted in quite different magnetic properties. Thus this PCM effect might be more pronounced in film form.

Chapter 5

Conclusion

In conclusion, the magnetic phase change and its recovery in cobalt oxides $PrBaCo_2O_{5.5}$ was successfully obtained by an appropriate heat treatment. This phase change may be considered as a potential phase-change memory effect. It employs the switching between the oxygen-vacancy ordered and the disordered phases, and the two phases have different magnetic properties. Thus this effect can be expressed as a phase-change magnetic memory effect.

Investigations of the two phases displayed that the disordered phase showed a superparamagnetic behavior, in sharp contrast to the ordered phase with a ferromagnetic behavior. Transport properties showed that the ordered phase had a sharp metal-insulator transition, which was broadened in the disordered phase. Structural analysis revealed that partial disorder had been generated through the phase-change process. The change of magnetism in the disordered phase was attributed to this structural change.

A similar magnetic phase change was also obtained in $TbBaCo_2O_{5.5}$ by the same heat treatment. But the observed disordering effect was a mixed effect of both the vacancy disorder and the influence of oxygen content.

Consequently, this study has worked on the phase control of strongly correlated systems. The phase control performed in this study realized the in-situ state switching, and it is advantageous for applications compared to other conventional phase-control methods. Although the memory effect proposed in this work has not been optimized for its working conditions, it is believed that the control of disorder in strongly correlated systems will provide a new exploring stage of the phase-change memory effect.

References

[1] Hard Disk Basics, *HowStuffWorks*. (http://computer.howstuffworks.com/hard-disk1.htm)

[2] IBM 350 disk storage unit, *IBM*. (http://www-03.ibm.com/ibm/history/exhibits/storage/storage_350.html)

[3] What is an External Hard Drive? *wiseGEEK*. (http://www.wisegeek.com/what-is-an-external-hard-drive.htm)

[4] Toshiba Leads Industry in Bringing Perpendicular Data Recording to HDD, *Toshiba: Press Releases*, 14 December, 2004. (http://www.toshiba.co.jp/about/press/2004_12/pr1401.htm)

[5] *Yesky*, February 23, 2006. (http://diy.yesky.com/harddisk/279/2313779_2.shtml)

[6] Flash Memory: Tunneling and Erasing, *HowStuffWorks*. (http://electronics.howstuffworks.com/flash-memory1.htm)

[7] Fujio Masuoka: Thanks For The Memory, *BusinessWeek*. (http://www.businessweek.com/magazine/content/06_14/b3978021.htm?chan=global biz_asia_today%27s+top+story)

[8] *LogFS*, May 15, 2007. (http://lwn.net/Articles/234441/)

[9] S. R. Ovshinsky, *Phys. Rev. Lett.* **21** (1968) 1450: Reversible electrical switching phenomena in disordered structures.

[10] J. Feinleib, J. DeNeufville, S. C. Moss, and S. R. Ovshinsky, *Appl. Phys. Lett.* **18** (1971) 254: Rapid reversible light-induced crystallization of amorphous semiconductors.

[11] A. Kolobov, P. Fons, A. Frenkel, A. Ankudinov, J. Tominaga, and T. Uruga, *Nature Materials* **3** (2004) 703: Understanding the phase-change mechanism of reweitable optical media.

[12] A. V. Kolobov, P. Fons, J. Tominaga, A. I. Frenkel, A. L. Ankudinov, S. N. Yannopoulos, K. S. Andrikopoulos, and T. Uruga, *Jpn. J. Appl. Phys.* **44** (2005) 3345: Why Phase-Change Media Are Fast and Stable: A New Approach to an Old Problem.

[13] A. V. Kolobov, P. Fons, J. Tominaga, T. Uruga, *J. Non-Cry. Sol.* **352** (2006) 1612: Why DVDs work the way they do: The nanometer-scale mechanism of phase change in Ge-Sb-Te alloys.

[14] Intel to Sample Phase Change Memory This Year, *DailyTech*, March 9, 2007. (http://www.dailytech.com/article.aspx?newsid=6371)

[15] A Memory Breakthrough, *Technology Review*, February 04, 2008. (http://www.technologyreview.com/Infotech/20148/?a=f)

[16] K. Conder, E. Pomjakushina, A. Soldatov, and E. Mitberg, *Mater. Res. Bull.* **40** (2005) 257: Oxygen content determination in perovskite-type cobaltates.

[17] M. Karppinen, M. Matvejeff, K. Salomaki, and H. Yamauchi, *J. Mater. Chem.* **12** (2002) 1761: Oxygen content analysis of functional perovskite-derived cobalt oxides.

[18] D. Akahoshi, and Y. Ueda, *J. Solid State Chem.* **156** (2001) 355: Oxygen Nonstoichiometry, Structures, and Physical Properties of $YBaCo_2O_{5+x}$ ($0.00 \leq x \leq 0.52$).

[19] J. C. Burley, J. F. Mitchell, S. Short, D. Miller, and Y. Tang, *J. Solid State Chem.* **170** (2003) 339: Structural and Magnetic Chemistry of $NdBaCo_2O_{5+\delta}$.

[20] P. S. Anderson, C. A. Kirk, J. Knudsen, I. M. Reaney, and A. R. West, *Solid State Sci.* **7** (2005) 1149: Structural Characterization of $REBaCo_2O_{6-\delta}$ phases (*RE* = Pr, Nd, Sm, Eu, Gd, Tb, Dy, Ho).

[21] I. A. Leonidov, M. V. Patrakeev, E. B. Mitberg, O. N. Leonidova, and V. L. Kozhevnikov, *Inorg. Mater.* **42** (2006) 196: Thermodynamic and Structural Properties of $PrBaCo_2O_{5+\delta}$.

[22] Md. Motin Seikh, Ch. Simon, V. Caignaert, V. Pralong, M. B. Lepetit, S. Boudin, and B. Raveau, *Chem. Mater.* **20** (2008) 231: New Magnetic Transitions in the Ordered Oxygen-Deficient Perovskite $LnBaCo_2O_{5.50+\delta}$.

[23] A. Maignan, C. Martin, D. Pelloquin, N. Nguyen, and B. Raveau, *J. Solid State Chem* **142** (1999) 247: Structural and Magnetic Studies of Ordered Oxygen-Deficient Perovskites $LnBaCo_2O_{5+\delta}$, Closely Related to the 112 Structure.

[24] X. S. Wu, H. L. Zhang, J. R. Su, C. S. Chen, and W. Liu, *Phys. Rev. B* **76** (2007) 094106: Internal friction study of the phase transition in $GdBaCo_2O_{5+\delta}$ bulk materials.

[25] A. A. Taskin, A. N. Lavrov, and Yoichi Ando, *Phys. Rev. Lett.* **90** (2003) 227201: Ising-Like Spin Anisotropy and Competing Antiferromagnetic-Ferromagnetic Orders in $GdBaCo_2O_{5.5}$ Single Crystals.

[26] A. A. Taskin, A. N. Lavrov, and Yoichi Ando, *Phys. Rev. B* **71** (2005) 134414: Transport and magnetic properties of $GdBaCo_2O_{5+x}$ single crystals: A cobalt oxide with square-lattice CoO_2 planes over a wide range of electron and hole doping.

[27] V. P. Plakhty, Yu. P. Chernenkov, S. N. Barilo, A. Podlesnyak, E. Pomjakushina, E. V. Moskvin, and S. V. Gavrilov, *Phys. Rev. B* **71** (2005) 214407: Spin structure and magnetic phase transitions in $TbBaCo_2O_{5.5}$.

[28] Yu. P. Chernenkov, V. P. Plakhty, V. I. Fedorov, S. N. Barilo, S. V. Shiryaev, and G. L. Bychkov, *Phys. Rev. B* **71** (2005) 184105: X-ray diffraction study of superstructure of $GdBaCo_2O_{5.5}$.

[29] F. Fauth, E. Suard, V. Caignaert, and I. Mirebeau, *Phys. Rev. B* **66** (2002) 184421: Spin-state ordered clusters in the perovskite $NdBaCo_2O_{5.47}$.

[30] M. Sota, Y. Yasui, T. Fujita, T. Miyashita, M. Sato and K. Kakurai, *J. Phys. Soc. Jpn.* **72** (2003) 1729: Magnetic Structures of High Temperature Phases of $TbBaCo_2O_{5.5}$.

[31] M. Soda, Y. Yasui, Y. Kobayashi, T. Fujita, M. Sato, and K. Kakurai, *J. Phys. Soc. Jpn.* **75** (2006) 104708: Existence of Co^{3+} Low-Spin State in $TbBaCo_2O_{5.5}$.

[32] M. Itoh, Y. Nawata, T. Kiyama, D. Akahoshi, N. Fujiwara, and Y. Ueda, *Physica B* **329-333** (2003) 751: Local magnetic properties and spin state of $YBaCo_2O_{5.5}$: ^{59}Co NMR study.

[33] H. Kubo, K. Zenmyo, M. Itoh, N. Nakayama, T. Mizota, and Y. Ueda, *J. Magn. Mag. Mater.* **272-276** (2004) 581: NMR study of ^{59}Co nuclei in $EuBaCo_2O_{5+x}$ ($x = 0$ and 0.5).

[34] S. Streule, A. Podlesnyak, D. Sheptyakov, E. Pomjakushina, M. Stingaciu, K. Conder, M. Medarde, M. V. Patrakeev, I. A. Leonidov, V. L. Kozhevnikov, and J. Mesot, *Phys. Rev. B* **73** (2006) 094203: High-temperature order-disorder transition and polaronic conductivity in $PrBaCo_2O_{5.48}$.

[35] S. Streule, A. Podlesnyak, E. Pomjakushina, K. Conder, D. Sheptyakov, M. Medarde, and J. Mesot, *Physica B* **378-380** (2006) 539: Oxygen order-disorder phase transition in $PrBaCo_2O_{5.48}$ at high temperature.

[36] M. Baran, V. I. Gatalskaya, R. Szymczak, S. V. Shiryaev, S. N. Barilo, K. Piotrowski, G. L. Bychkov, and H. Szymczak, *J. Phys.: Condens. Matter* **15** (2003) 8853: Magnetic phase transitions in $TbBaCo_2O_{5.5}$ single crystals.

[37] A. Podlesnyak, A. Karlin, K. Conder, E. Pomjakushina, M. Stingaciu, and P. Allenspach, *J. Magn. Mag. Mater.* **316** (2007) e710: Magnetic and electric transport properties of $TbBaCo_2O_{5.5}$ single crystal.

[38] Y. Moritomo, T. Akimoto, M. Takeo, A. Machida, E. Nishibori, M. Takata, M. Sakata, K. Ohoyama, and A. Nakamura, *Phys. Rev. B* **61** (2000) R13325: Metal-insulator transition induced by a spin-state transition in $TbBaCo_2O_{5.5}$.

[39] H. Kusuya, A. Machida, Y. Moritomo, K. Kato, E. Nishibori, M. Takata, M. Sakata, and A. Nakamura, *J. Phys. Soc. Jpn.* **12** (2001) 3577: Structural Change at Metal-Insulator Transition of $Tb_2Ba_2Co_4O_{11}$.

[40] C. Frontera, J. L. Garcia-Munoz, A. Llobet, and M. A. G. Aranda, *Phys. Rev. B* **65** (2002) 180405: Selective spin-state switch and metal insulator transition in $GdBaCo_2O_{5.5}$.

[41] C. Frontera, J. L. Garcia-Munoz, A. Llobet, M. A. G. Aranda, J. Rodriguez-Carvajal, M. Respaud, J. M. Broto, B. Raquet, H. Rakoto, and M. Goiran, *J. Alloys Comp.* **323-324** (2001) 468: Structural, spin state, and magnetic transitions in $GdBaCo_2O_{5+\delta}$ ($\delta \sim 0.5$).

[42] C. Frontera, J. L. Garcia-Munoz, A. E. Carrillo, M. A. G. Aranda, I. Margiolaki, and A. Caneiro, *Phys. Rev. B* **74** (2006) 054406: Spin state of Co^{3+} and magnetic transitions in $RBaCo_2O_{5.50}$.(R = Pr, Gd): Dependence on rare-earth size.

[43] C. Frontera, J. L. Garcia-Munoz, A. E. Carrillo, and A. Caneiro, *J. Magn. Mag. Mater.* **316** (2007) e731: Spin state and magnetic interactions of Co^{3+} in $PrBaCo_2O_{5.5}$.

[44] C. Frontera, A. Caneiro, A. E. Carrillo, J. Oro-Sole, and J. L. Garcia-Munoz, *Chem. Mater.* **17** (2005) 5439: Tailoring Oxygen Content on $PrBaCo_2O_{5+\delta}$ Layered Cobaltites.

[45] S. Streule, A. Podlesnyak, J. Mesot, M. Medarde, K. Conder, E. Pomjakushina, E. Mitberg, and V. Kozhevnikov, *J. Phys.: Condens. Matter.* **17** (2005) 3317: Effect of oxygen ordering on the structural and magnetic properties of the layered perovskites $PrBaCo_2O_{5+\delta}$.

[46] A. Podlesnyak, S. Streule, M. Medarde, K. Conder, E. Pomjakushina, and J. Mesot, *Physica B* **359-361** (2005) 1348: Effect of oxygen nonstoichiometry on structural and magnetic properties of $PrBaCo_2O_{5+\delta}$.

[47] C. Frontera, J. L. Garcia-Munoz, O. Castano, C. Ritter, and A. Caneiro, *J. Phys.: Condens. Matter.* **20** (2008) 104228: The effect of oxygen disorder on magnetic properties of $PrBaCo_2O_{5.50}$.layered cobaltite.

[48] C. Frontera, J. L. Garcia-Munoz, and O. Castano, *J. Appl. Phys.* **103** (2008) 07F713: Influence of R-ion size on spin state of Co and magnetic properties of $RBaCo_2O_{5.50}$. cobaltites.

Acknowledgement

It has been almost two years since I first came to this laboratory. As a foreign student starting life and study here, so many people have helped me throughout the time, and without them I could not even have continued my study. Hence I would like to thank all the people who have helped me in this work.

First of all, I would like to express my best gratitude to Prof. H. Takagi who offered me such an opportunity of studying at University of Tokyo. His guidance has been very important and helpful to the whole course of my study.

I would like to thank Prof. M. Nohara, who has given me many suggestions in my study, as well as Dr. Y. Nakamura and Dr. A. Yamamoto, who have given me so much help in my experiment.

I would like to make a grateful acknowledgement to Dr. T. Takayama, who has instructed and advised me all along, from experimental technique to academic writing and presentation skills. This work could not have been done without his instructions.

I am also thankful to the following people for their help in everyday study and life: Dr. S. Takashima, Dr. K. Fujiwara, Dr. N. Katayama, Dr. T. Suzuki, Dr. H. Kuriyama, Dr. S. Pyon, Dr. H. Tomita, Dr. T. Yajima, Dr. D. Hirai, Mr. L. Kobayashi, Mr. T. Nemoto, Mr. K. Yamaguchi, Y. Konno, R. Matsumura, R. Nomura, S. Oikawa, K. Satoh, M. Toko, and so on.

Finally, I would like to express my acknowledgement to all the people who helped me in my study and life in this laboratory.

GU Yunpeng

July 15, 2008